8G93-F

APPLICATION OF ITOS AND NIMBUS INFRARED MEASUREMENTS TO MAPPING SEA ICE

FINAL REPORT

CONTRACT No.1-36025
JUNE 1972

JAMES C. BARNES
DAVID T. CHANG
JAMES H. WILLAND

prepared for

DEPARTMENT OF COMMERCE
NATIONAL OCEANIC AND ATMOSPHERIC ADMINISTRATION
NATIONAL ENVIRONMENTAL SATELLITE SERVICE

ARA ALLIED RESEARCH ASSOCIATES, INC.
HAMMONDS FERRY ROAD, BALTIMORE, MD. 21203

8G93-F

APPLICATION OF ITOS AND NIMBUS INFRARED MEASUREMENTS TO MAPPING SEA ICE

FINAL REPORT

CONTRACT No.1-36025
JUNE 1972

JAMES C. BARNES
DAVID T. CHANG
JAMES H. WILLAND

prepared for

DEPARTMENT OF COMMERCE
NATIONAL OCEANIC AND ATMOSPHERIC ADMINISTRATION
NATIONAL ENVIRONMENTAL SATELLITE SERVICE

ARA ALLIED RESEARCH ASSOCIATES, INC.
HAMMONDS FERRY ROAD, BALTIMORE, MD. 21203

FOREWORD

The research described in this report was performed for the National Oceanic and Atmospheric Administration under Contract No. 1-36025 to Allied Research Associates, Inc. (ARA). The work was completed by the authors at Environmental Research & Technology, Inc. (ERT) under a subcontract with Allied Research Associates. The report was printed by ARA.

The authors wish to acknowledge the technical assistance provided throughout the study by Dr. E. Paul McClain, of the National Environmental Satellite Service, Environmental Sciences Group. The ITOS data were provided by the National Environmental Satellite Service, and the Nimbus data were obtained through the courtesy of the Nimbus-ATS Data Utilization Center (NADUC) of the National Aeronautics and Space Administration. Mr. C. James Bowley, of ERT, assisted in the preparation of the report.

ABSTRACT

The application to ice mapping of recently available ITOS and Nimbus thermal infrared data is investigated. The ITOS-1 Scanning Radiometer (SR) and the Nimbus-4 Temperature-Humidity Infrared Radiometer (THIR) have been the first satellite high resolution sensors to operate in the 10.5-12.5 μm spectral interval. In this study, arctic ice distributions are mapped from ITOS Direct Readout (DRSR) imagery; densitometric analyses are performed using DRSR and Nimbus imagery; ITOS digitized temperatures are mapped through the 5-level scheme developed in previous studies; and the use of Nimbus daytime IR data is evaluated.

The results of the investigations show that the ITOS DRSR imagery is particularly useful for ice mapping because of the reduced noise content achieved through direct readout transmission. Furthermore, the densitometric measurements indicate that crude quantitative information on types of ice conditions can be derived from these data. Evidence is also found that the combined use of IR and visible data may provide more information on ice conditions than can be deduced from either type of data alone. At least during wintertime, the 5-level mapping scheme appears to be applicable to the ITOS measurements.

The analysis of the Nimbus THIR measurements reveals that during the summer season subtle temperature differences between ice and water may not be noticeable in the gray-scale data display. During periods of alternating daylight and darkness, however, a relationship is found between the diurnal variation in IR temperature and ice thickness and/or amount. This parameter can, therefore, be used to assist in the interpretation of ice features, and offers promise as a tool for objective interpretation of ice and clouds.

TABLE OF CONTENTS

LIST OF ILLUSTRATIONS

LIST OF ILLUSTRATIONS (contd.)

1. INTRODUCTION

1.1 Purpose of Study

The potential of satellite infrared data for sea-ice survey has been established through studies carried out in the past few years. Until recently, however, the only relatively high-resolution infrared measurements were those of the Nimbus High Resolution Infrared Radiometer (HRIR) in the 3.4 to 4.2 μm spectral interval. Now, the ITOS and most recent Nimbus spacecraft have provided high-resolution measurements in the 10.5 to 12.5 μm thermal infrared spectral interval. The purpose of the research described in this report is to study the application to ice mapping of the recently available data, particularly the measurements from the ITOS Scanning Radiometer (SR).

The current study has three principal objectives: (1) to determine whether ice distributions can be mapped from nighttime ITOS-SR data using the techniques and thresholds developed previously for Nimbus HRIR data; (2) to perform quantitative analyses of the ITOS-SR photofacsimile (pictorial) data; and (3) to compare nighttime and daytime thermal infrared measurements using ITOS and Nimbus data.

1.2 Previous Studies

The overall application of earth satellites for ice survey has been summarized in a recent paper by McClain and Baliles (1971). Techniques to use Nimbus HRIR data for mapping sea-ice distributions have been developed in studies by Barnes, Chang, and Willand (1969, 1970, 1972). The results of these previous studies have shown that principal sea-ice boundaries can be reliably mapped from nighttime HRIR photofacsimile film strips.

A particularly encouraging result of the Nimbus-3 analyses is that ice mapping in the Arctic appears to be the most reliable during the winter months of December and January, because of the greater occurrence of cloud-free conditions and the accumulation of thicker ice. Since winter is the season of maximum polar darkness, it is the period when other data sources are severely limited.

Even though extremely useful information can be derived from HRIR film strips in their existing format, limitations do exist. In fact, the results of previous densitometric analyses have indicated that quantitative measures of either the absolute effective blackbody temperature or the relative gradients of these temperatures cannot be derived from the film-strip data even when the gray-scale step wedges are used as reference. Gray-scale enhancement experiments have demonstrated, however, that the present photofacsimile presentations may be improved upon by using discrete steps in the gray scale and by limiting the number of gray scales used. The format which permits the greatest accuracy in visual interpretation is the binary mode. In this mode, a scan spot is mapped in either of two tones, black or white, depending on whether or not its value falls below, or is equal to or exceeds, a preassigned threshold value. Thus, this form of data presentation permits accurate quantitative interpretations, although the total information content of the interpretation is only the accurate positioning of the isoline represented by the threshold value.

The results of the earlier enhancement experiments have shown that the information content of the interpretation can be increased by increasing the number of discrete gray levels. The gray levels must be readily distinguishable, however, since the purpose of the display is to reduce ambiguity by

matching the information content of the display with the information content of the interpretation. In a series of subjective tests, a five gray-scale display was found to be optimum in that more accurate interpretations of the temperatures could be obtained and the depiction of significant features enhanced (Barnes, Chang, and Willand, 1972).

1.3 Data Sample

The data sample used in this study consists of measurements from the ITOS-1 and Nimbus-4 satellites. ITOS-1 was launched in February 1970 and operated until June 1971; because of interference problems, however, much of the Scanning Radiometer (SR) data prior to December 1970 were too noisy to be of use. The Nimbus-4 Temperature-Humidity Infrared Radiometer (THIR) was in nearly continuous operation from early April 1970 until early April 1971.

The THIR and SR thermal infrared channels operated in the 10.5 to 12.5 μm spectral interval. Since these were the first satellite high-resolution radiometers to operate in the longer wavelength atmospheric window, in which solar contamination is negligible, Nimbus-4 and ITOS-1 were the first satellites to provide both nighttime and daytime thermal infrared data. A more complete description of the two sensors and the data formats is presented in Section 2 of this report.

The data analyzed are primarily from the Baffin Bay and Beaufort Sea areas, although some analyses are also performed for orbital passes covering the Bering Sea, Hudson Bay, and the Kara Sea. Nimbus and ITOS photographs are used to assist in the interpretation of the infrared measurements.

2. DISCUSSION OF THERMAL INFRARED MEASUREMENTS

2.1 Nimbus THIR Data

The Nimbus 4 Temperature-Humidity Infrared Radiometer (THIR) is a two-channel scanning radiometer. One of the channels, with spectral response located between 6.5 and 7.0 μm is useful for estimating the mean upper tropospheric water vapor content. The other channel has a spectral response between 10.5 and 12.5 μm. This channel is located in the atmospheric water vapor window between the ozone absorption band at 9.6 μm and the carbon dioxide band at 15 μm. The purpose of this second channel is to provide a measure of the surface emitted radiation (i.e., the surface of the earth or of a cloud top).

The optical design of the THIR is in many respects similar to that used for the High Resolution Infrared Radiometers (HRIR) of the earlier Nimbus spacecraft. Cross-track spatial coverage is achieved by means of a rotating mirror, and through an arrangement using a beam-splitter and separate detectors,measurements in both channels can be made simultaneously. However, the optical design of the filter-detector module is such that each of the detectors looks through a different set of optics. Hence, whereas the optical axes of the channels are identical, the instantaneous fields-of-view (IFOV) are quite different. Due to energy (and therefore detectability) considerations, the 6.5 to 7.0 μm channel has an IFOV of about 21 milliradians. At the nominal Nimbus orbital altitude of 1112 km (600 n.mi.), this IFOV corresponds to a ground resolution of about 21 km at nadir. The 10.5 to 12.5 μm channel is designed with a much smaller IFOV of approximately 7.0 milliradians. At the same orbital altitude, the ground

resolution at nadir is about 6.7 km., which is a small improvement over the 8.5 km value of the earlier Nimbus radiometer.

Data from the Nimbus THIR are available in essentially the same formats as were the earlier HRIR data. For use in this study, the 10.5 to 12.5 μm channel measurements were acquired in both the photofacsimile film-strip and digitized formats. The digitized temperature values were mapped in a 1:2 million polar stereographic projection, a scale that had not been available with earlier Nimbus data. At polar latitudes, the digitized value printed out at each grid point generally represents the average of some 10 to 20 single resolution elements. Full-resolution data listings were also used in some analyses.

2.2 ITOS SR Data

The ITOS-1 Scanning Radiometer (SR) is also a two-channel radiometer. One channel measures in the 10.5 to 12.5 μm interval, whereas the other measures in the visible portion of the spectrum at 0.52-0.73 μm. As with the Nimbus system, spatial coverage of the earth is achieved by cross-track scanning in conjunction with the along-track motion of the spacecraft, and measurements in both channels can be obtained simultaneously through the use of a beam-splitter and separate detectors. With this arrangement, however, each of the channels has a different instantaneous field-of-view (IFOV). For the visible channel, the IFOV results in a ground resolution at nadir of about 3.7 km. In the case of the 10.5 to 12.5 μm channel, the ground resolution is degraded to about 7.4 km.

Measurements in the 10.5 to 12.5 μm channel were used in the current study. From a theoretical point of view, these data are identical to those obtained by the 10.5 to 12.5 μm channel of the Nimbus-4 THIR. Consequently,

the interpretation of both sets of measurements are based on the same physical principles. In practice, however, the measurements from these two radiometers over the same target area may be quantitatively different, as a result of differences in sensor characteristics or calibration procedures.

With regard to calibration of the ITOS measurements, two components of the problem must be considered. The first is the electronic component, which is in the ground equipment; the second is the thermal component, which has to do with the spacecraft itself. Short-term variations in the electronic component may be significant, such that the calibration can even vary from pass-to-pass. Information from NOAA/NESS indicated that neither component was being properly incorporated into the ITOS calibration procedures during the period of the data sample used in this study. Thus, without an external correction, the absolute temperature values measured by the ITOS Scanning Radiometer cannot be regarded as being correct. However, the relative values measured on any particular pass are still useful.

In the ITOS direct readout (DRSR) imagery examined in this study, the total temperature range (about 180°K to 310°K) is displayed in a linear table of 32 steps. In this presentation, each gray level represents a temperature interval of 4°K. For purposes of ice mapping, DRSR images received at the Wallops and Fairbanks ground stations were obtained. The Wallops range of reception extends far enough north to cover the southern Baffin Bay area. The Fairbanks images, which were from a limited sample, cover an area extending from the Aleutian Islands northward across Alaska and extending to northernmost Greenland. Because of noise contamination, the usefulness of the Fairbanks sample was somewhat reduced.

The ITOS-SR taped data are available in a mapped projection at a scale of about 1:4 million. In this format the data are essentially full-resolution. Each data point is presented in alphanumeric code, and represents a range of temperature rather than an absolute value. In most instances the maps were printed in two temperature tables: in the first, the temperature range represented by each code figure is 4^{o} for values less than $260^{o}K$, 2^{o} for values between 260^{o} and $280^{o}K$, and 4^{o} for values greater than $280^{o}K$; in the second, the range for each code figure is $2^{o}K$, with the data cut off at an upper limit of $273^{o}K$. The majority of the analyses were performed using the first table, in which the temperature breakdown is not too different from that of the DRSR imagery.

The application of ITOS infrared data in meteorological analysis and forecasting is discussed in a report by Anderson and Smith (1971). In this report, a more thorough description of the Scanning Radiometer and the data formats is presented.

2.3 Considerations for Ice Mapping

The application to ice mapping of measurements made in the 3.4 to 4.2 μm spectral interval by earlier Nimbus spacecraft is discussed in detail in previous studies by Barnes, Chang, and Willand (1969, 1970). As was true with the shorter wavelength measurements, the output of the 10.5 to 12.5 μm channels of both the Nimbus-4 and ITOS-1 radiometers is specified in terms of an effective blackbody temperature (T_{bb}). In the thermal infrared data, therefore, the T_{bb} measured over a cloud-free region provides a first estimate of the actual surface temperature. For a surface with an emissivity of unity and in the absence of any atmospheric attenuation, the T_{bb} is in

fact the surface temperature. Since for all surfaces, emissivity, ε, is less than or equal to one, and the atmosphere above the surface attenuates the surface emitted radiance, it can be expected that in general the measured effective temperature, T_{bb}, is lower than the actual surface temperature. Experiences with the earlier HRIR data (e.g. Smith et al, 1970) suggest that a discrepancy of 2 to 3^{o}K, with the T_{bb} being the lower value, would not be unexpected.

Operation of the radiometers in the 10.5 to 12.5 μm thermal infrared channel represents an improvement over the 3.4 to 4.2 μm channel as far as surface temperatures are concerned. Measurements in the long wavelength window can be made even during daylight hours without interference from reflected and scattered solar radiation, thus providing measurements of surface emitted energy during both the daylight and nighttime portions of each orbital pass. Day and night surface temperature measurements were not previously possible because of solar contamination at the shorter wavelength.

3. APPLICATION OF ITOS DRSR IMAGERY TO ICE MAPPING

3.1 Analysis of DRSR Thermal Patterns

Thermal patterns were mapped for several of the ITOS DRSR images received at the Wallops and Fairbanks Stations. The Wallops data sample was during the period from late December 1970 through early April 1971; the Fairbanks sample was during March 1971. The DRSR images were analyzed using the techniques developed in previous studies of Nimbus HRIR film-strips. Cloud-free areas were established through identification of geographic landmarks, and ice boundaries were mapped where maximum thermal gradients were observed. Often, continuity from pass to pass confirmed the locations of ice boundaries. Although the DRSR images were not geographically gridded, a sufficient number of landmarks could be identified in most instances to permit accurate mapping.

An ITOS DRSR pass received at Wallops station on 25 February 1971 is shown in Figure 3-1a. A Nimbus IDCS photograph of the same area, taken one month later when sufficient illumination existed, is shown in Figure 3-1b. The DRSR image, which extends to about 70^{o}N, is representative of the northernmost coverage achievable at a station located at Wallop's latitude (38°N). Northern Baffin Bay, Ungava Bay, and southern Baffin Island are prominent in the image (see Map, Figure 3-2). At this season, land areas, including the smaller islands, appear colder than the sea ice.

Despite the interval of a month, the ice boundary in Baffin Bay and along the Labrador Coast remains nearly unchanged in the two observations. On both dates considerable low stratus cloud exists over the ice-free water. In the thermal image the cloud cover exhibits essentially the same gray tone

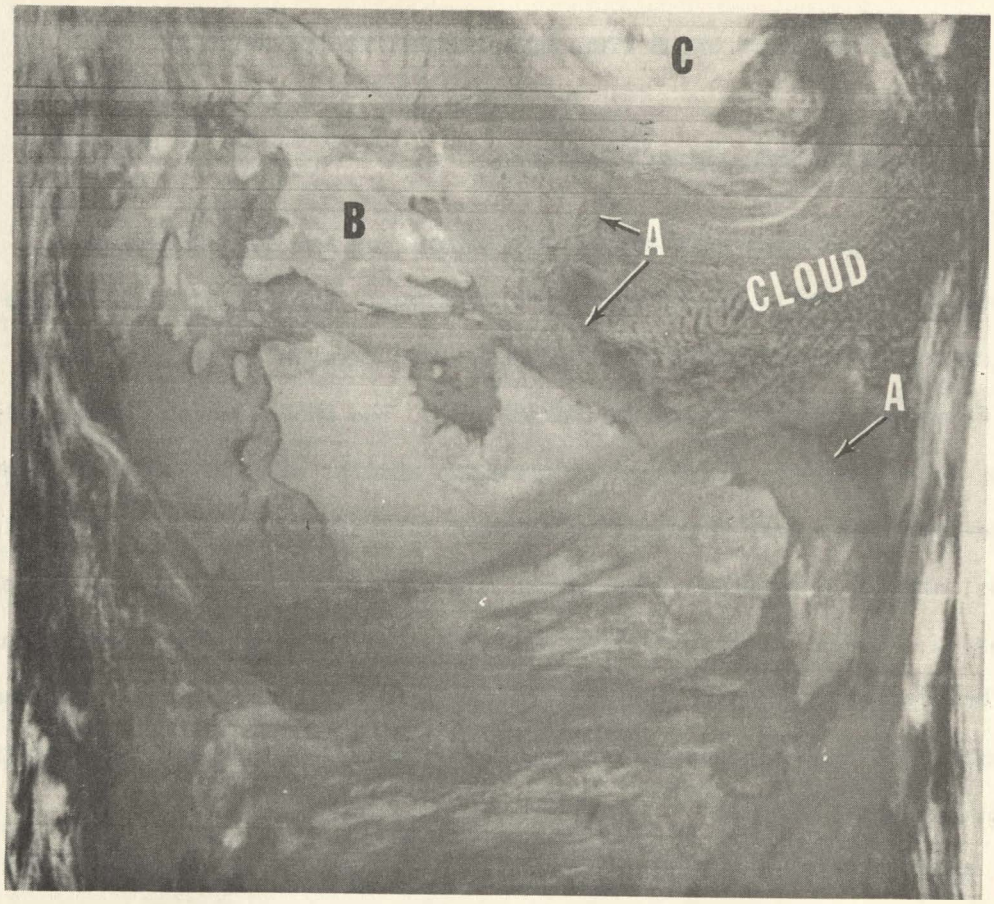

Figure 3-1a ITOS-1 Nighttime DRSR image showing area from northeastern Canada to Baffin Bay, 25 February 1971. The ice edge (A) is separated from the stratus cloud by a narrow darker (warmer) band. Baffin Island is at B; Greenland (C) is partially cloud covered.

Figure 3-1b Nimbus 4 IDCS photograph showing same area as in Figure 3-1a, 26 March 1971. The ice edge is at A; Baffin Island (B) and Hudson Bay (C) can be identified.

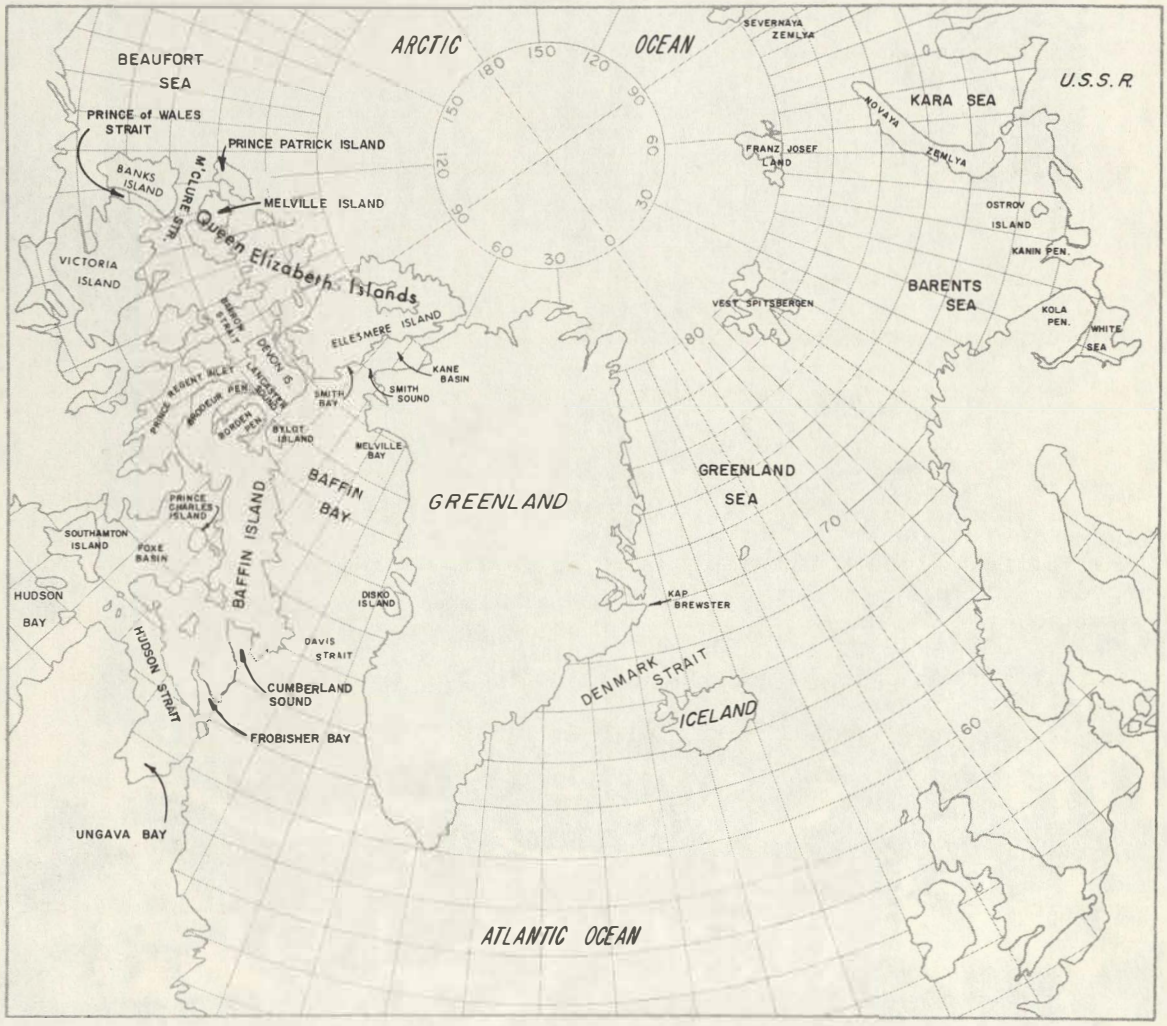

Figure 3-2 Map of Arctic region

(temperature range) as the ice. As was often true with the earlier Nimbus data, however, the ice boundary can be identified because of a narrow warm band separating ice and cloud (see Barnes, Chang, and Willand, 1972).

In the original DRSR print, considerable detail in the ice cover can be seen. Darker patterns (warmer areas) are evident near most of the smaller islands such as those in Hudson Bay and Akpatok Island in Ungava Bay, and along the coast of Baffin Island such as in Cumberland Sound and Frobisher Bay. Striations in the Baffin Bay ice extending eastward from Baffin Island can also be seen. Similar darker (warmer) patterns in Baffin Bay and near the various islands appear in images received and other dates as well. Furthermore, in the photograph shown in Figure 3-1b and in other photographs shown in Section 4 of this report, striations can be seen in the Baffin Bay ice and areas of lower reflectance occur near islands and in some inlets. Because of the consistency of the patterns in both the thermal imagery and the photographs, these are deduced to be either areas of thinner ice or, more likely, areas of lesser ice concentrations.

In Figure 3-3a, an example of a DRSR pass received at Fairbanks is given. An ITOS AVCS photograph taken 12 hours earlier on the same date, 11 March, 1971, is given in Figure 3-3b. In both the IR and visible images the Alaskan Coast and the Aleutian Islands can be identified, indicating that the area is essentially cloud-free except for low stratus over the ocean. Just south of the Aleutians, "wakes" in the stratus exist as a result of the wind flow over the individual islands.

Despite the noise problem, ice features are detectable in the DRSR data. The ice edge mapped in the Bering Sea is in close agreement with the ice edge mapped from the photograph, and many smaller scale features

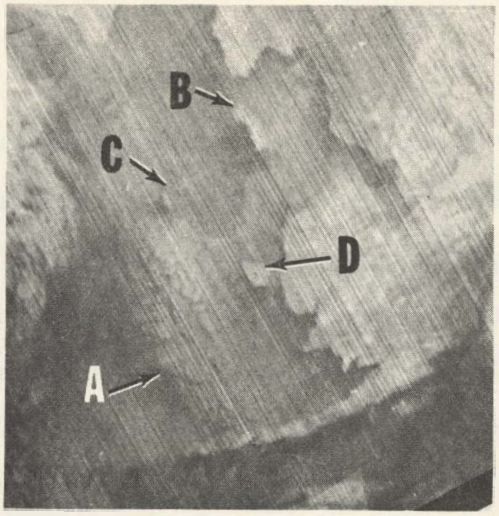

(a) Nighttime DRSR

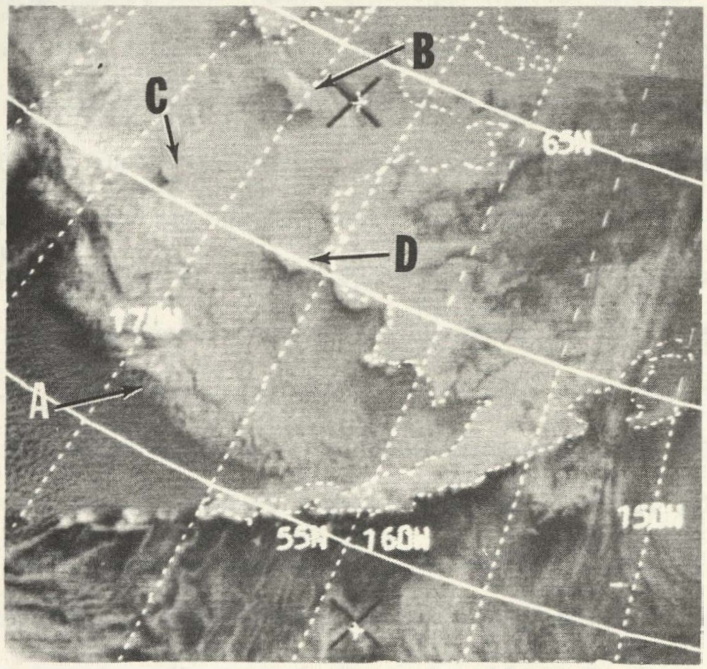

(b) AVCS

Figure 3-3 ITOS-1 DRSR image and AVCS photograph showing ice distribution in the Bering Sea, 11 March 1971. The ice edge is at A; St. Lawrence (B), St. Matthew (C), and Nunivak (D) Islands can be identified.

within the ice pack seen in the photograph can also be detected in the original DRSR print. In the eastern part of the Bering Sea, a well-defined thermal gradient extends from St. Lawrence to Nunivak Island and then westward toward St. Matthew Island. (Fig.3-3b). Because this gradient is detectable in DRSR imagery on the following two days as well (data not shown), it is almost certainly associated with a real ice feature. In the corresponding visible data (Fig. 3-3b), however, no significant change in brightness is evident, as is the case in the area along the southern side of St. Lawrence Island. Thus, the thermal gradient is deduced to be associated with the edge of thicker ice or the edge of ice with a greater amount of snow cover, but not with a boundary separating different ice concentrations.

In the Fairbanks imagery, excellent detail is also evident in the area as far east as northernmost Greenland. In some passes (not shown), a persistent narrow, warm band extends from off Ellesmere Island to Prince Patrick Island. Also, some of the fiords of northern Ellesmere Island that are detectable in the DRSR imagery are of the order of three miles in width, a smaller distance than the nominal 4.5 mile spatial resolution of the Scanning Radiometer.

3.2 Concurrent ITOS DRSR and Nimbus THIR Imagery

On several of the dates for which ITOS DRSR images from Wallops Station were acquired, Nimbus film strips covering the same area were also available. Passes over Hudson Bay about three hours apart on 14 January are shown in Figure 3-4 (a and b). These figures illustrate that in general the Nimbus-4 film strips contain a much greater amount of noise than do the ITOS-1 DRSR images. Although principal features such as Foxe Basin,

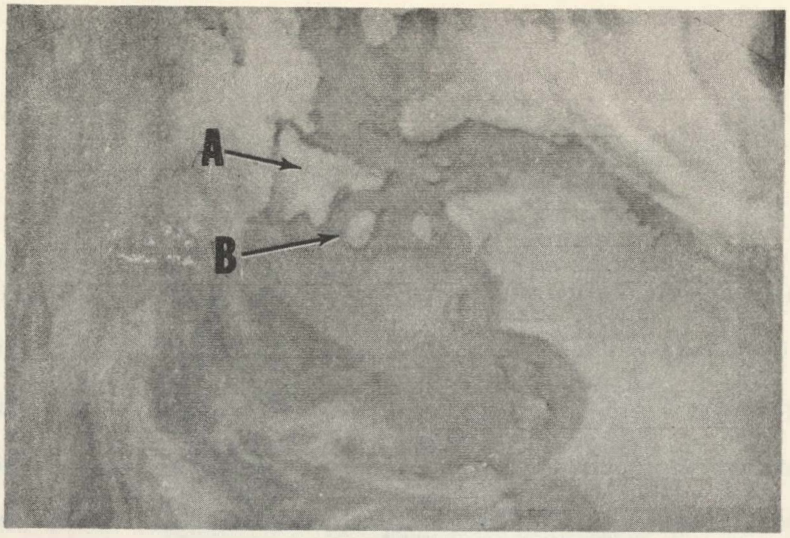

Figure 3-4a ITOS-1 Nighttime DRSR image showing northern Hudson Bay and Foxe Basin, 14 January 1971. Southampton Island is at A and Coats Island at B.

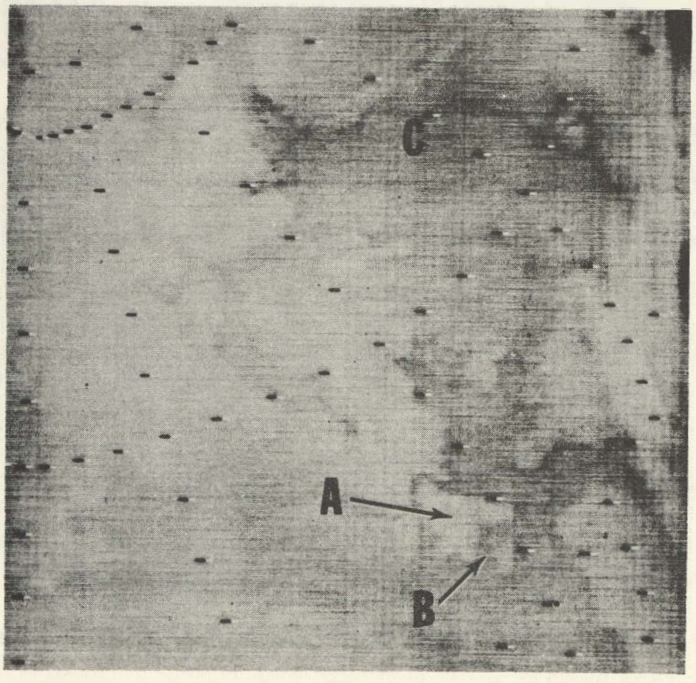

Figure 3-4b Nimbus-4 Nighttime THIR film strip showing area from northern Hudson Bay to northern Baffin Bay, 14 January 1971. Southampton Island is at A, Coats Island at B, and Baffin Bay at C.

Baffin Island, and Southampton Island can be seen in the Nimbus film strip, the smaller scale features, clearly evident in the ITOS imagery, are obscured.

Some Nimbus-4 film strips, as shown elsewhere in this report, are less noisy than the 14 January data. However, none of the Nimbus film-strips was found to be as noise-free as the best of the ITOS DRSR images (we have information that direct readout THIR data received from early Nimbus-4 passes were also of excellent, noise-free quality; because of power limitations, however, very little Nimbus-4 DRIR was transmitted thereafter). The comparison between ITOS direct readout and Nimbus taped data demonstrates the potential for acquiring measurements with reduced data noise through direct readout transmission.

3.3 Densitometric Analysis

3.3.1 Nimbus-4 Film Strips

To obtain a quantitative evaluation of the direct readout infrared data, densitometric analyses were performed using both the ITOS DRSR imagery and Nimbus film strips. Since similar analyses had been performed previously using the Nimbus HRIR data (Barnes, Chang, and Willand, 1972), the Nimbus-4 film strips were analyzed first in the current study. Also, the Nimbus photofacsimile film strip format includes a 10-level gray-scale calibration wedge, in which each step corresponds to an effective blackbody temperature as specified in The Nimbus-4 User's Guide (Sabatini, 1970). A comparable calibration wedge was not included with the DRSR data.

Density measurements were made, using positive transparencies of selected orbital passes, to determine:

1. The pass-to-pass variabilities in gray-scale step wedge densities as depicted in "controlled" processed photofacsimile data.
2. The effective blackbody temperature range or ranges corresponding to the largest spatial density changes.
3. The feasibility of using densitometric values to map quantitatively sea ice features.

The Nimbus-4 orbital passes selected for analysis are from the late spring and early summer of 1970. During this period, the temperature difference between ice and water is small, providing more of a test of the gray-scale format to depict features of low contrast. The dates analyzed and the densities corresponding to each of the gray-scale steps measured from the positive transparencies are shown in Table 3-1. Since the measurements were made with a relatively low resolution transmission densitometer, the densities were read only to the nearest tenth.

The data in Table 3-1 show a relatively high degree of variability in densities between passes, with the difference in density for any of the steps ranging from a low value of 0.2 to a high value of 0.5. The large values of density difference appear to be associated with higher values in density. These data indicate that quantitative interpretation of the photofacsimile data, in terms of effective blackbody temperature without reference to a simultaneously exposed step wedge, could lead to erroneous results.

A second distinct feature in the measured densities is the non-linear relationship between increments in density and increments in gray-scale step number. The greatest differences in density between adjacent steps ($\Delta D = 0.2$) are found between steps 4 and 7. Between steps 1 and 2 and

steps 9 and 10, the density differences are generally of the order of ≤ 0.1. The two exceptions are passes 281N and 348N; in the former, ΔD for steps 1 and 2 is 0.3, and in the latter, ΔD for steps 9 and 10 is 0.2.

The observed non-linearity between density and step number does not necessarily imply a similar nonlinearity between density and effective temperature, since the relationship between effective temperature and step number is also non-linear. Based on the "calibration" data contained in

TABLE 3-1
GRAY-SCALE STEP-WEDGE DENSITY MEASUREMENTS
OF SELECTED NIMBUS-4 PASSES

		Gray Scale Step Number									
Pass No.	Date	1	2	3	4	5	6	7	8	9	10
252N	27-4-70	2.1	2.0	1.8	1.6	1.4	1.3	1.0	0.9	0.8	0.8
281N	29-4-70	1.0	1.6	1.4	1.3	1.1	0.9	0.8	0.7	0.6	0.6
322N	2-5-70	2.0	1.9	1.7	1.5	1.3	1.2	1.0	0.9	0.7	0.7
348N	4-5-70	2.1	2.0	1.8	1.6	1.4	1.2	1.0	0.9	0.8	0.6
471N	13-5-70	2.1	2.1	1.9	1.7	1.5	1.4	1.1	1.0	0.9	0.8
Mean Value		2.0	1.9	1.7	1.5	1.4	1.2	1.0	0.9	0.8	0.7
Minimum Value		1.9	1.6	1.4	1.3	1.1	0.9	0.8	0.7	0.6	0.6
Maximum Value		2.1	2.1	1.9	1.7	1.5	1.4	1.1	1.0	0.9	0.8

the User's Guide, the density data in Table 3-1 were converted to the effective blackbody temperatures plotted in Figure 3-5. Each of the curves may be considered to be a calibration chart for the corresponding orbit's photofacsimile data. Additionally, the curves show the temperature resolution of the facsimile format, where resolution is defined by $R = (\Delta D/\Delta T_{bb})$, with

ΔD being an increment in density and ΔT_{bb} the corresponding increment in effective blackbody temperature. As R increases, a given value of ΔD, such as that defined by some visual threshold, will depict smaller values of ΔT_{bb}, thus providing a format more suitable for visual discrimination between features of low temperature contrast.

The graphs shown in Figure 3-5 suggest that R is non-linearly dependent on T_{bb}. Figure 3-6 shows a graph of the dependence of R on T_{bb} computed from values of ΔD averaged for the five passes previously shown in Table 3-1. It is clear from this figure that for the five passes selected, the gray-scale presentation was fortuitously optimized for the depiction of ice boundaries (T_{bb} between 265 and 275^{o}K) and for warm water features (T_{bb} > 290^{o}K). For these features the temperature resolution is better than .01/^{o}K.

The calibration curves shown in Figure 3-5 were applied to the temperature interpretation of a number of density measurements made of ice features in the photofacsimile data from the five orbits. Only three features were selected - Ice Cap, Solid Pack Ice and Open Water. It was felt that these features are sufficiently distinct such that little or no ambiguity should be involved in their identification. The results of the density measurements in terms of the inferred blackbody temperatures are shown in Table 3-2.

In terms of the threshold temperature values previously established by Barnes, Chang and Willand (1972) for the Nimbus-2 data, these inferred temperatures are certainly reasonable. The suggestion here is that while it might be difficult to obtain precise measurements of temperature from the facsimile data, it is possible to use the data in quantitative and objective analysis for the identification of certain geophysical features.

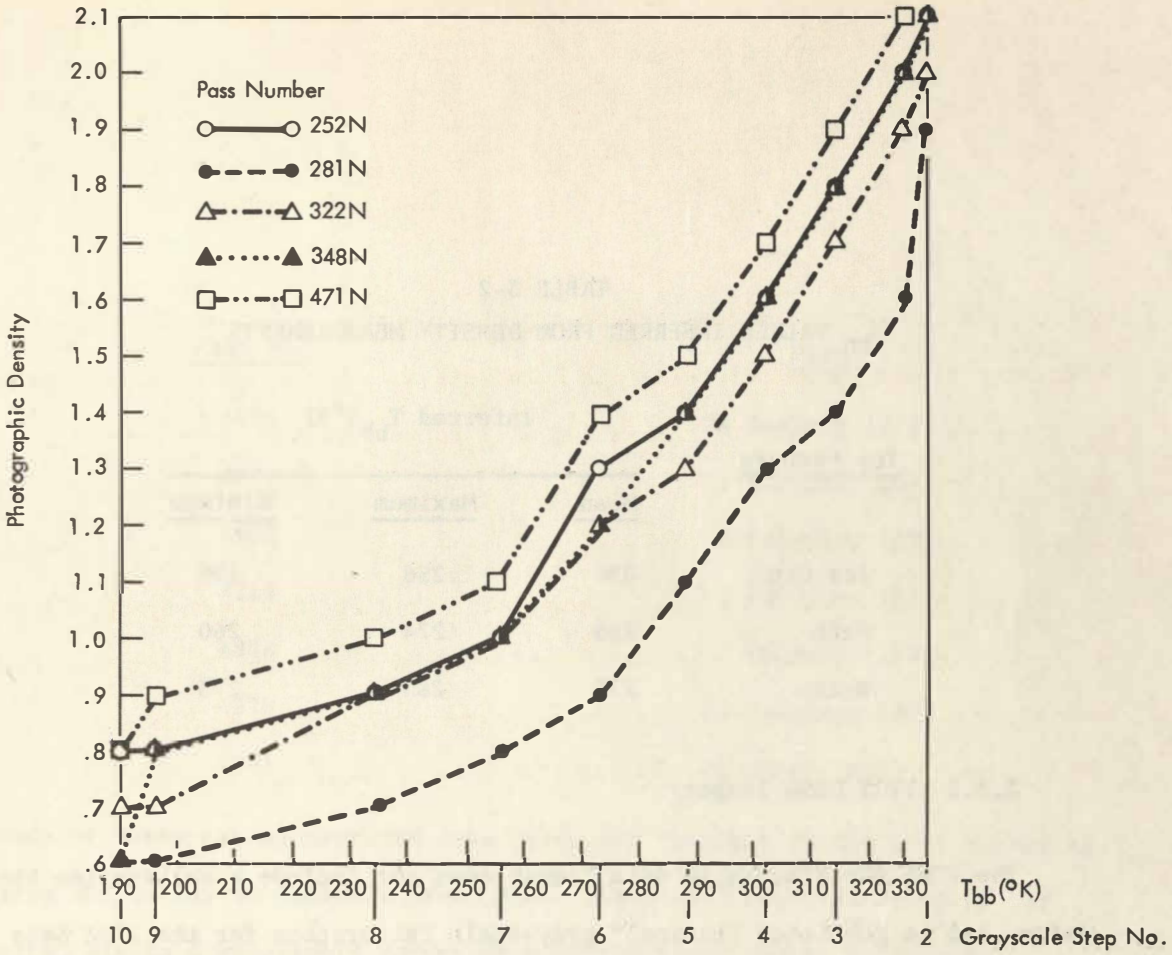

Figure 3-5 Graph showing photographic density vs. effective blackbody temperature (T_{bb}) for five Nimbus-4 nighttime THIR film strips in April and May 1970.

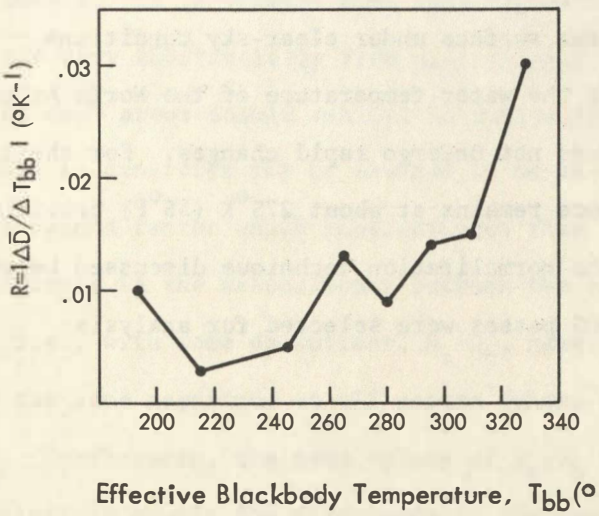

Figure 3-6 Graph showing relationship between R (where $R = |\Delta\bar{D}/\Delta T_{bb}|$) and effective blackbody temperature for Nimbus-4 THIR film strips, derived from calibration curves shown in Figure 3-5.

TABLE 3-2

T_{bb} VALUES INFERRED FROM DENSITY MEASUREMENTS

Ice Feature	Inferred T_{bb} (°K)		
	Mean	Maximum	Minimum
Ice Cap	234	256	196
Pack	266	274	260
Water	278	283	273

3.3.2 ITOS DRSR Imagery

The ITOS photofacsimile data format does not include a calibration step wedge, and no published "nominal" gray-scale calibration for the ITOS data exists. Furthermore, due to the photographic processing involved, pass-to-pass density changes in the positive transparencies are to be expected even though the received signals were identical. It is, therefore, necessary to devise some means of "normalizing" the density measurements, if they are to be compared. To accomplish this, use was made of the photographic density corresponding to the sea surface under clear-sky conditions. From climatology, it is known that the water temperature of the North Atlantic south of the Greenland coast does not undergo rapid changes. For the late winter season, this temperature remains at about 275°K (35°F) providing a nearly invariant point for the normalization technique discussed below.

The following ITOS passes were selected for analysis:

Pass No.	Date
4603	26 January 1971
4678	1 February 1971
4690	2 February 1971
4715	4 February 1971
4878	7 February 1971
4978	25 February 1971
5091	6 March 1971

Each of these passes provided some clear-sky coverage of the area extending from Hudson Bay to southern Greenland. Figure 3-7 contains a map of the area, giving a geographic referencing of the index number (1 to 59) identifying the points in the film strips for which density measurements were made, and giving the normal January boundary of the pack ice in the Davis Strait area.

Figure 3-8 shows a plot of the range of densities measured at each of the index points. It is evident from this figure that the density at any point can vary substantially from pass to pass. Since temperatures over "ice cap" areas should exhibit no substantial changes, the large variations in densities may be assumed to be an artifact in the data processing. A second factor which substantiates this conclusion is the fact that the differences in the measurements between two passes were found to be "systematic"; i.e., with some exceptions, $D_a - D_b$, have the same sign and approximately the same magnitude at all points (where a and b are two different passes). Furthermore, the mean values of $D_a - D_b$ for the sample points 1 to 59 approximately equals the difference in the measured densities over the sea surface for the same pairs of orbital passes.

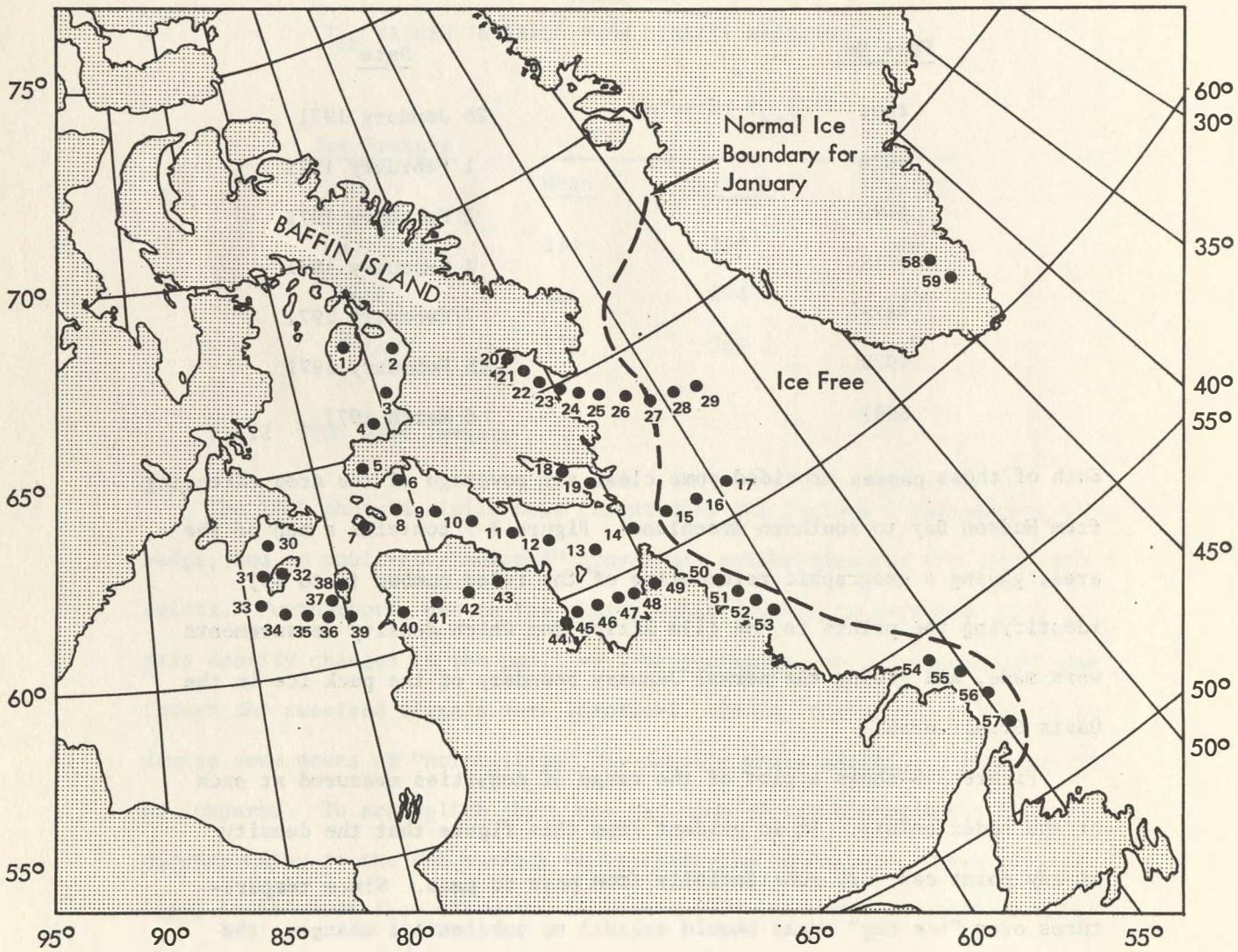

Figure 3-7 Map indicating locations of density measurements of ITOS-1 images.

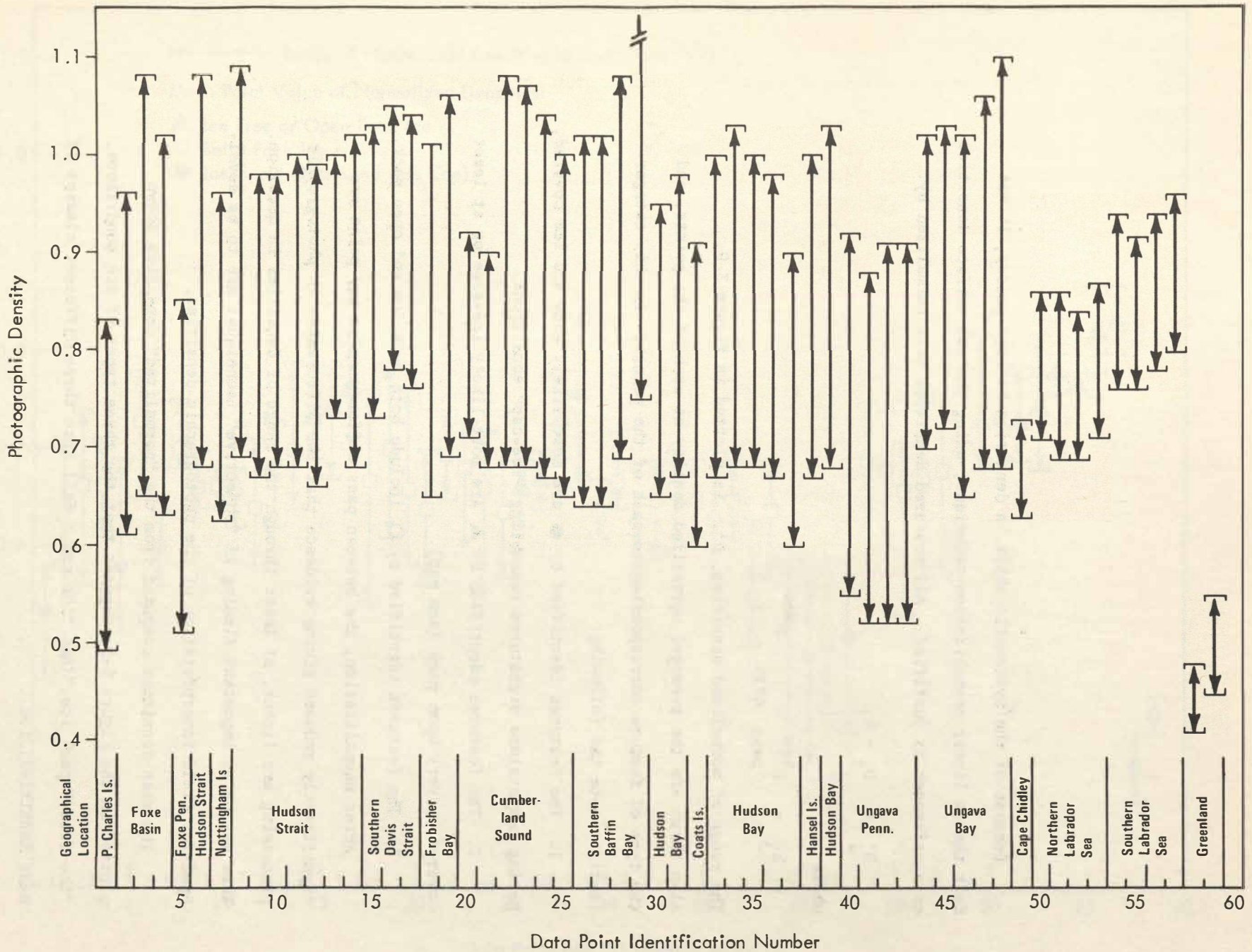

Figure 3-8 Graph showing range of density values measured at each data point shown in Figure 3-7. Sample consisted of seven ITOS-1 nighttime DRSR images.

Because of the systematic shift in densities between passes, it was felt that a linear normalization technique, using the sea surface densities as a reference is justified. All measured densities were normalized by:

$$D'_j = D_j + k_j$$

where

$$k_j = D^{sea}_{pass\ 4715} - D^{sea}_{j} .$$

The range of normalized densities, D', is plotted in Figure 3-9. Also shown are the averaged normalized density at each of the points, and the type of feature corresponding to each of the points. In this categorization, note the following:

1. The features identified by ● are most likely snow and ice covered, having temperature signatures resembling "ice-cap" conditions.

2. The features identified by ▲ are most likely ice-free or at least covered by very open pack (see map).

3. The features identified by □ include both pack ice and open pack.

After normalization, the between pass differences at any point are significantly reduced giving evidence that the differences in photographic processing are linear, at least through the range of densities in question. This may be an important finding if "objective" techniques are to be developed for field interpretation of the photographic densities.

The mean densities computed from the "normalized" densities shown plotted in the Figure 3-9, suggest that the three types of ice conditions, "ice-free," pack ice," and "ice cap," fall into three different classes of mean densities; i.e.,

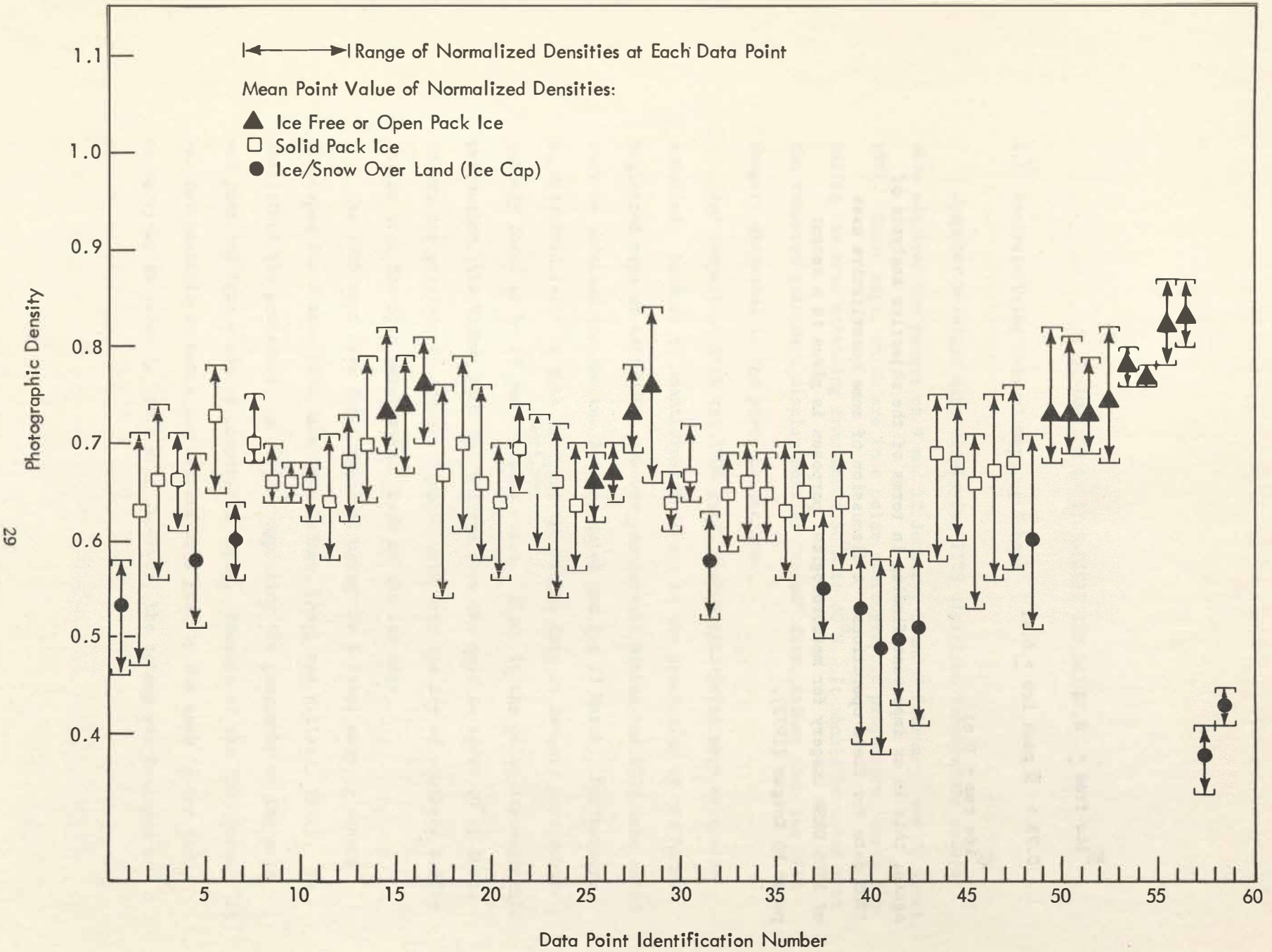

Figure 3-9 Graph showing range of normalized density values for same ITOS-1 DRSR data sample as shown in Figure 3-8.

$\overline{D}_{\text{ice-free}} \geq 0.73$

$0.73 > \overline{D}_{\text{pack ice}} \geq 0.61$

$\overline{D}_{\text{ice cap}} < 0.61$

Again, this is an important finding in terms of the objective analysis of ITOS data for field operations. A discussion of some quantitative uses of ITOS DRSR imagery for meteorological purposes is given in a recent paper by Keegan (1972).

4. EVALUATION OF ITOS DIGITIZED DATA

4.1 Analysis Using 5-Level Mapping Scheme

Computer printout maps displaying ITOS digitized temperature values were acquired for passes on 9 and 12 January, 5 and 7 February, and 27 March, 1971. These maps, which are in a polar stereographic projection, cover the Baffin Bay area extending from about 50^{o}N to 80^{o}N. It should be noted that the computer printouts display noisier "taped" data, rather than the DRSR imagery discussed in the previous section.

For comparison with the ITOS data, Nimbus grid-print maps were also acquired. Because of unanticipated delays in the processing of the Nimbus digitized maps at NASA/GSFC, however, concurrent Nimbus and ITOS data could only be obtained for the two January dates and for 27 March. Furthermore, as discussed later in this section, the Nimbus data in January were subsequently found to be of questionable value. Also, in the polar stereographic projection, the Nimbus maps only extend from the pole to about 70^{o}N; thus, it was not possible to compare temperatures over the ice of southern Baffin Bay or over the open water areas south of the ice edge.

The ITOS maps were first analyzed using the 5-level mapping scheme developed for Nimbus HRIR data (see Barnes, Chang and Willand, 1972). To facilitate the procedure, an overlay depicting the geography of the area was prepared from a map of comparable scale. Because of the ITOS format, it was not possible to match the temperatures exactly for each of the five categories; as shown in Table 4-1, however, the scheme was followed as closely as possible.

TABLE 4-1

FIVE-LEVEL MAPPING SCHEME USED IN ANALYSIS OF ITOS-SR DATA

Code Number	ITOS Temperature Range	Original Nimbus Temperature Range	Interpreted Features
1	$T \geq 274$	$T \geq 274$	Open water
2	$274 > T \geq 268$	$274 > T \geq 269$	Very open pack (1/10 - 3/10)
3	$268 > T \geq 264$	$269 > T \geq 264$	New ice, thin winter ice, or open pack (4/10 - 6/10)
4	$264 > T \geq 252$	$264 > T \geq 254$	Thick winter ice, polar ice, or close to compact pack (7/10 - 10/10)
5	$T<252$	$T<254$	Polar ice, ice cap, or winter land areas (snow covered)

The resulting temperature maps for Baffin Bay are shown in Figures 4-1 (a-e). The probable ice concentrations for each temperature range can be determined through reference to Table 4-1. During the wintertime dark period, few ice observations are available to correlate with the mapped temperatures. However, on 11-12 February, a few days after two of the analyzed passes, a Birds-Eye aerial reconnaissance was flown over Baffin Bay; the observed ice concentrations are plotted in Figure 4-2. On 27 March, a sufficient amount of illumination exists for a Nimbus AVCS photograph to be available. The photograph is shown in Figure 4-3, and the ice edge deduced from the visible data is plotted on the corresponding temperature map (Figure 4-1e).

On all five maps shown in Figure 4-1 the temperatures over Baffin Bay north of Davis Strait are indicative of close-to-compact or compact ice cover. The exception is in the "North Water" area near Smith Sound, where

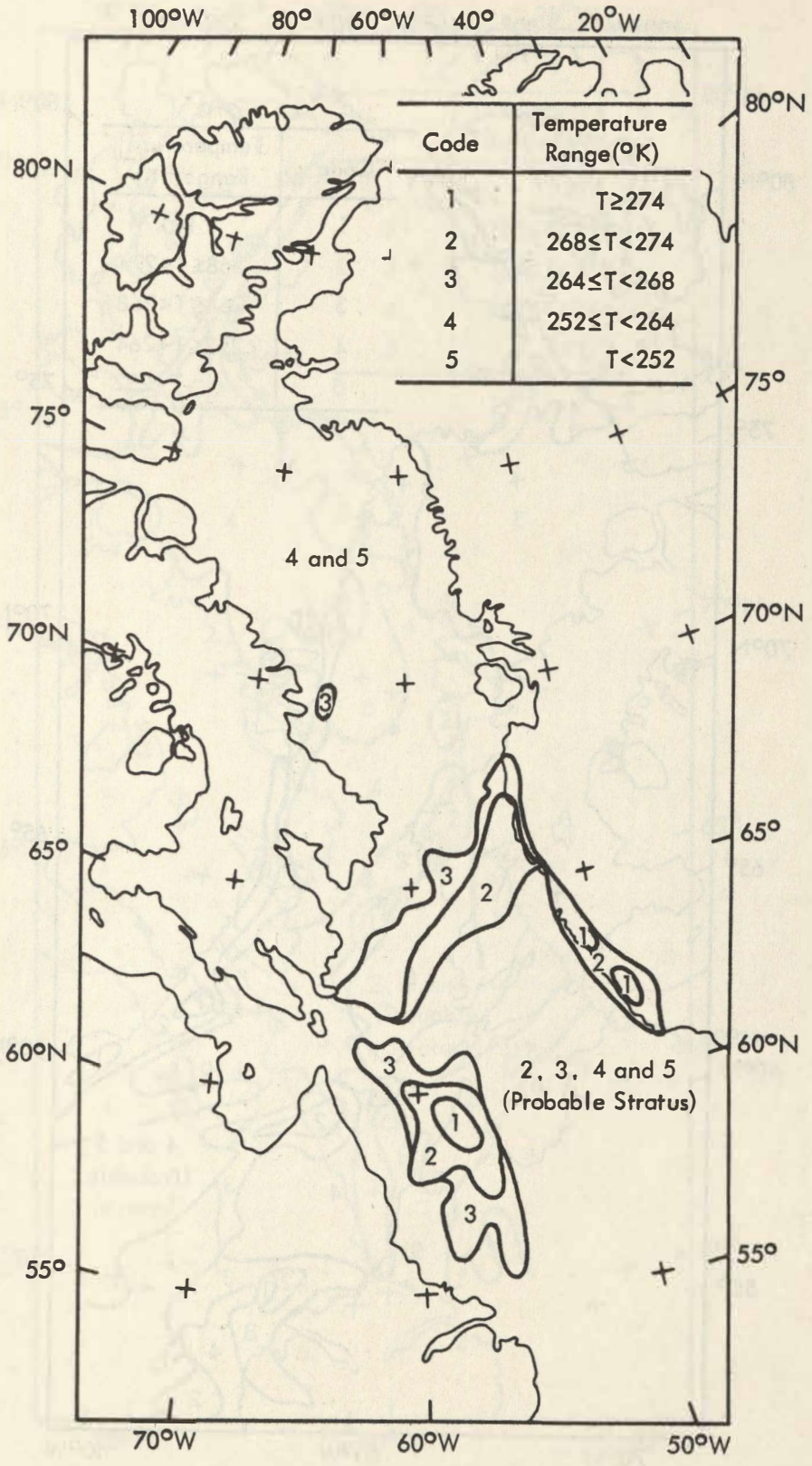

Figure 4-1a Temperature analysis from ITOS-1 digitized SR data, 9 January 1971.

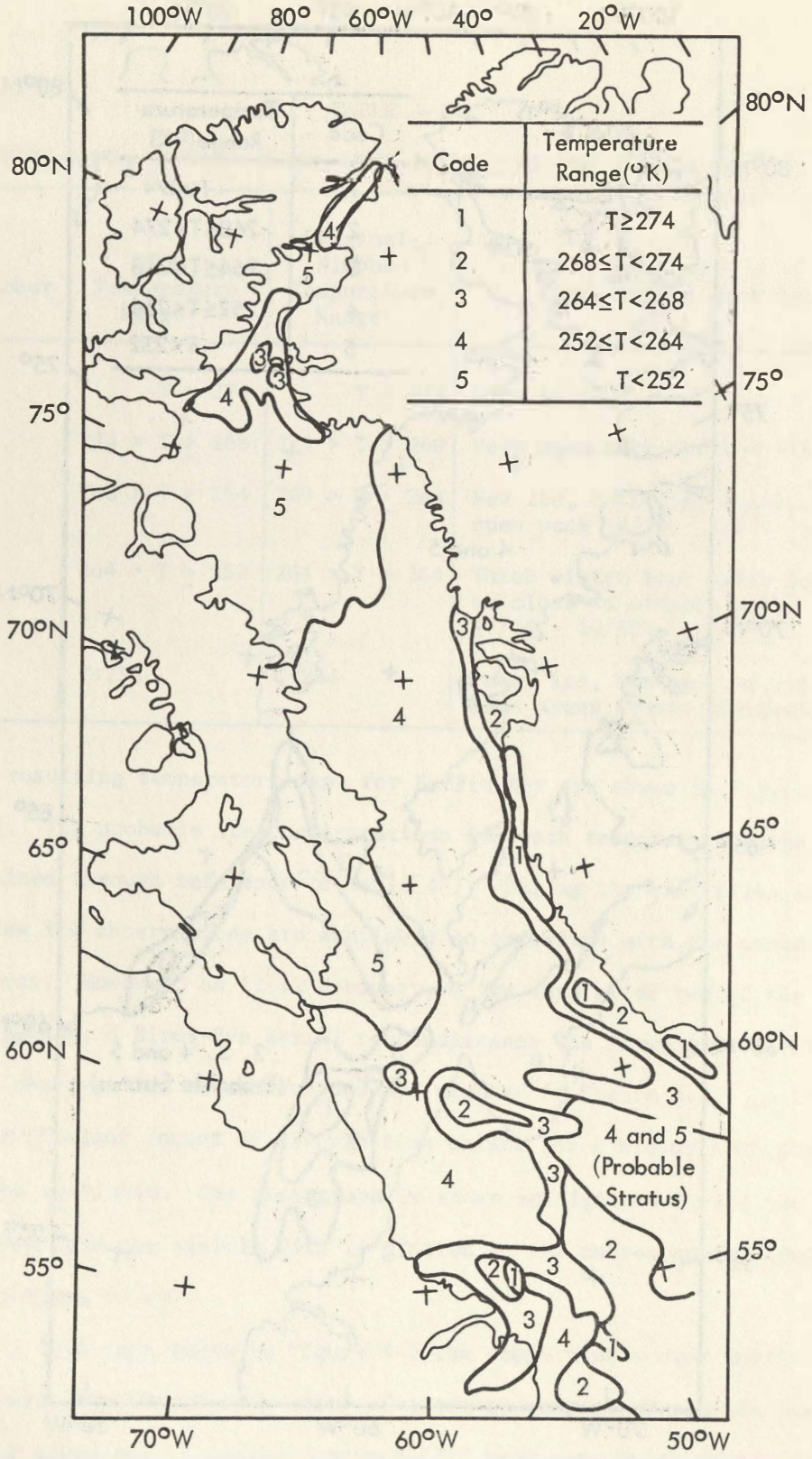

Figure 4-1b Temperature analysis from ITOS-1 digitized SR data, 12 January 1971.

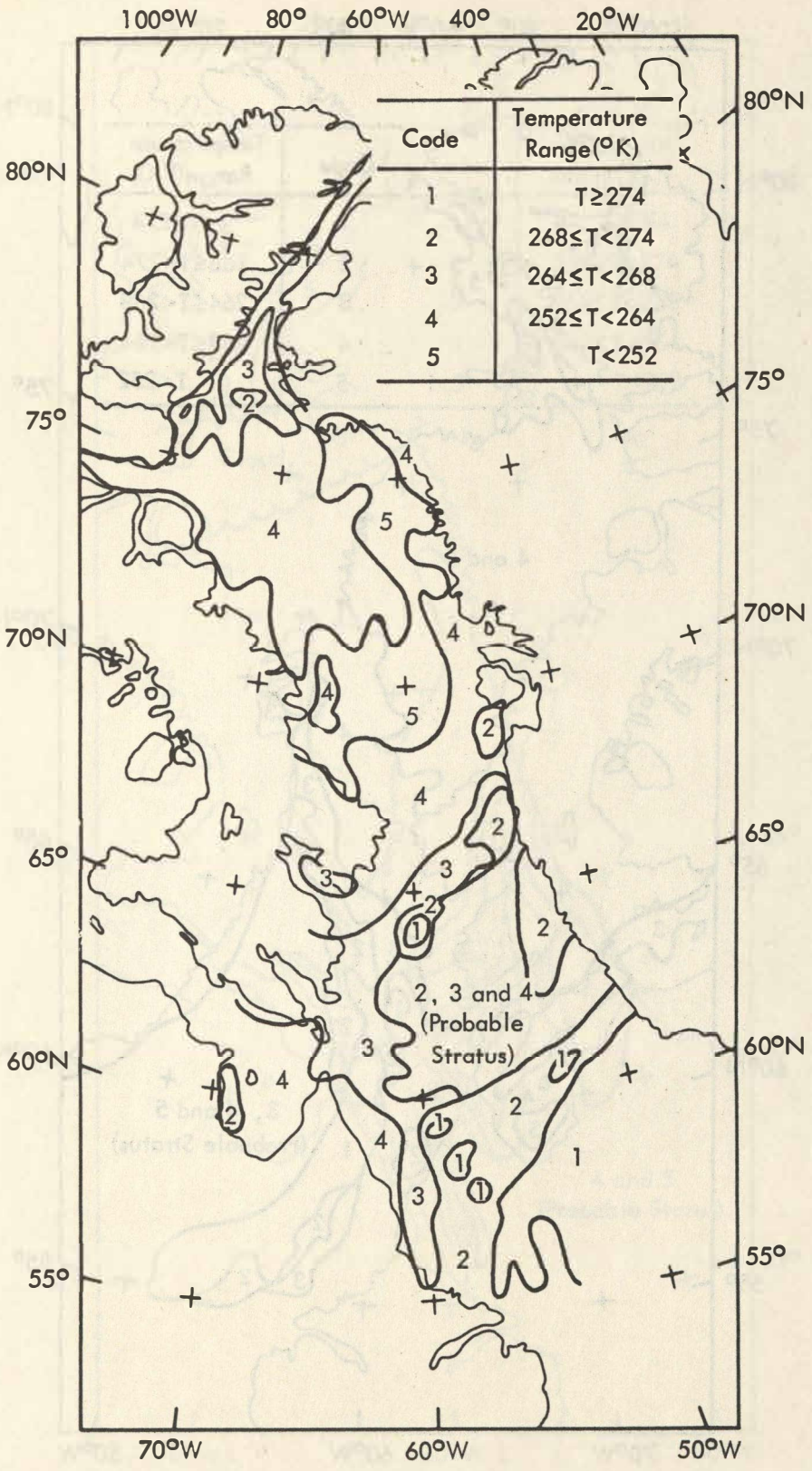

Figure 4-1c Temperature analysis from ITOS-1 digitized SR data, 5 February 1971.

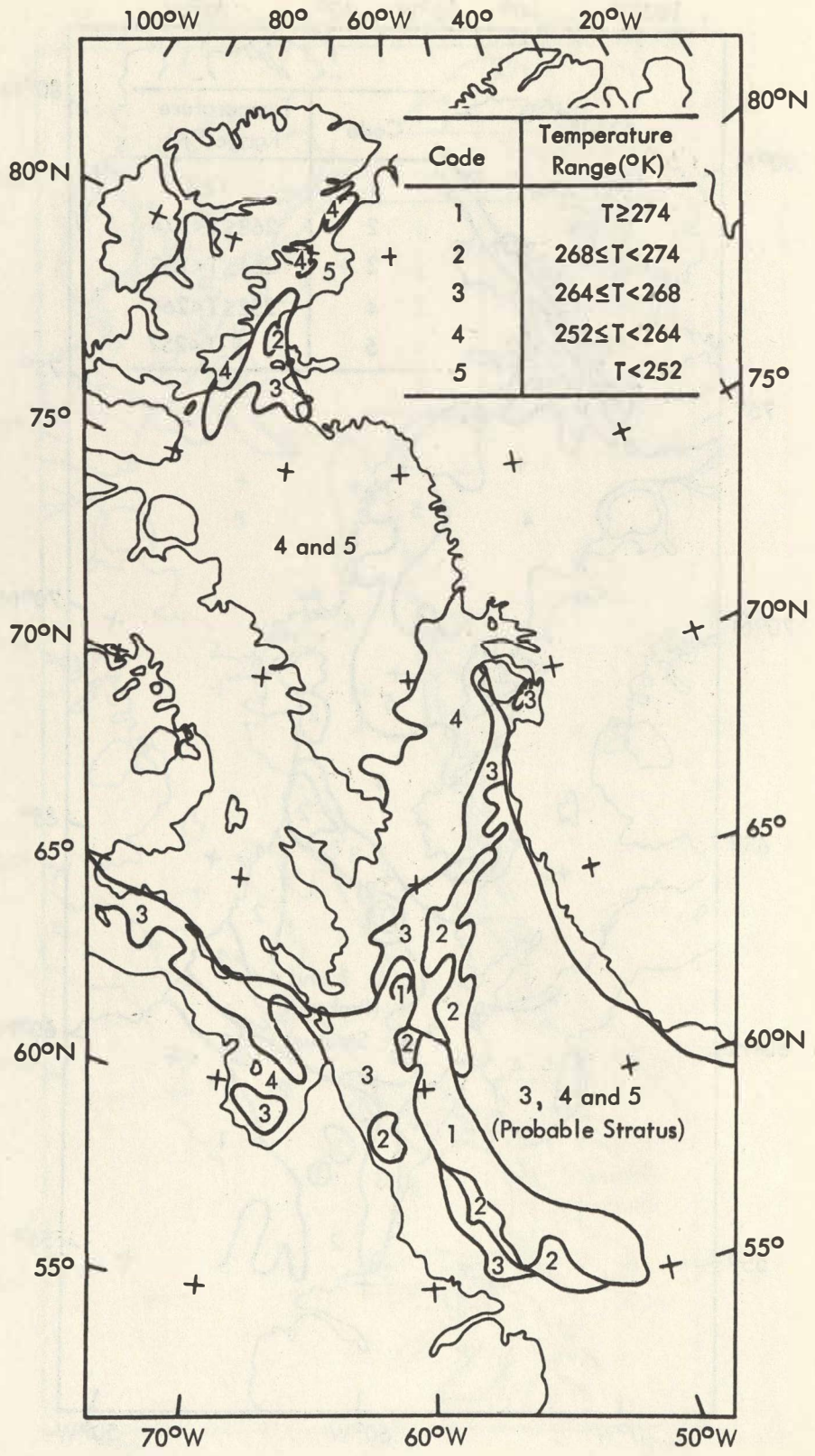

Figure 4-1d Temperature analysis from ITOS-1 digitized SR data, 7 February 1971.

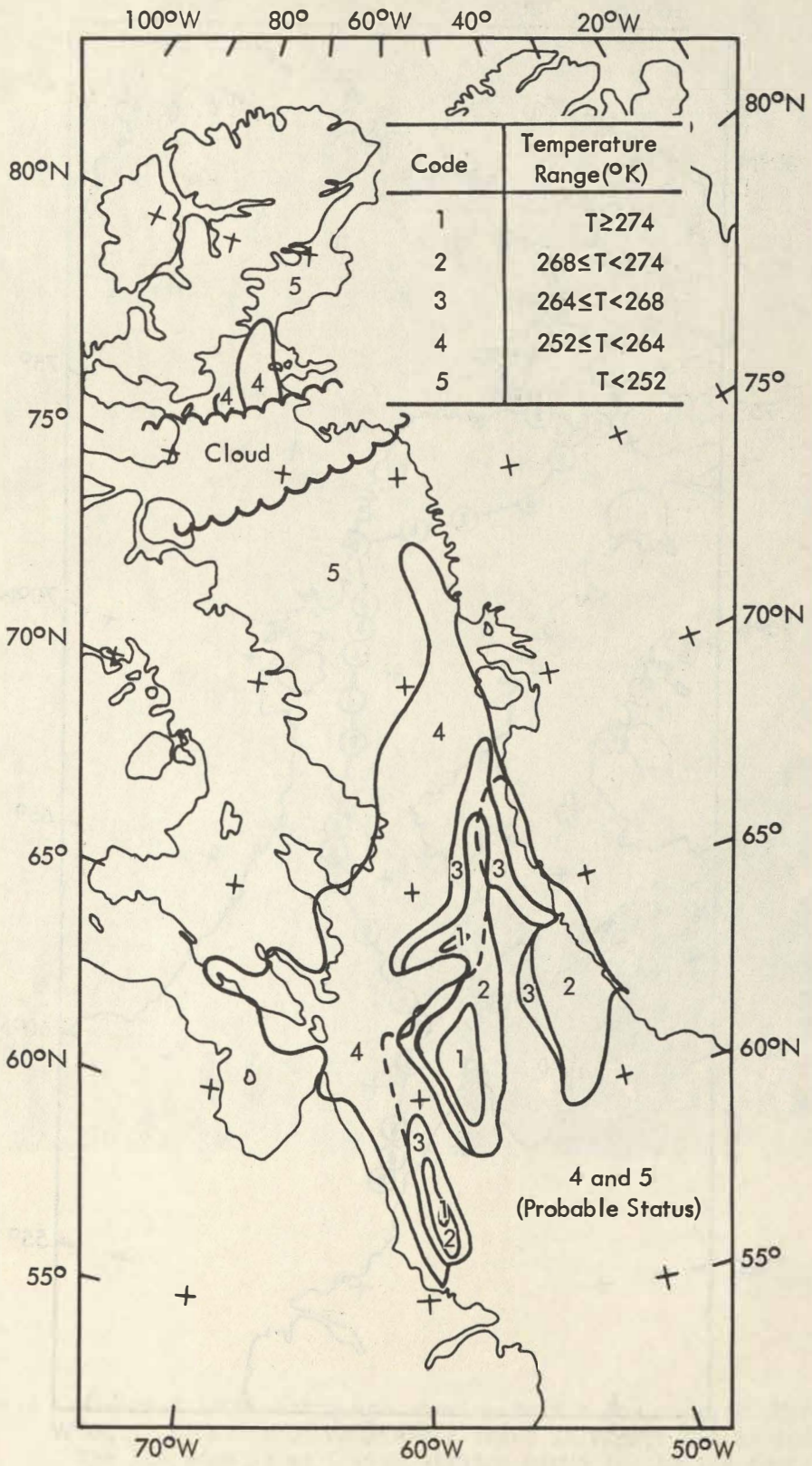

Figure 4-1e Temperature analysis from ITOS-1 digitized SR data, 27 March 1971. Heavy broken line indicates ice edge mapped from IDCS photograph on same date, shown in Figure 4-3.

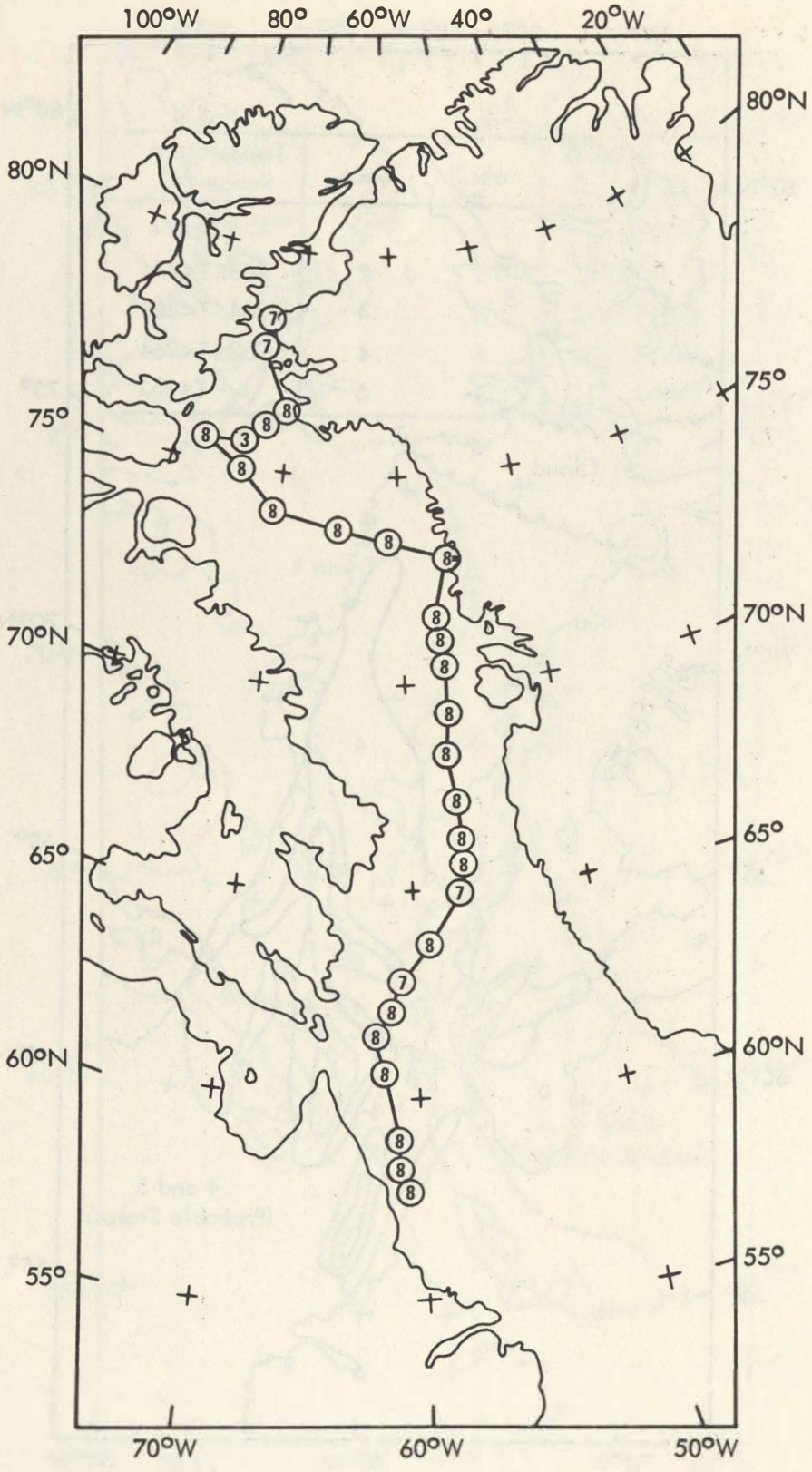

Figure 4-2 Ice concentrations (in oktas) observed on Birds-Eye flight, 11-12 February 1971 (Naval Oceanographic office, 1971).

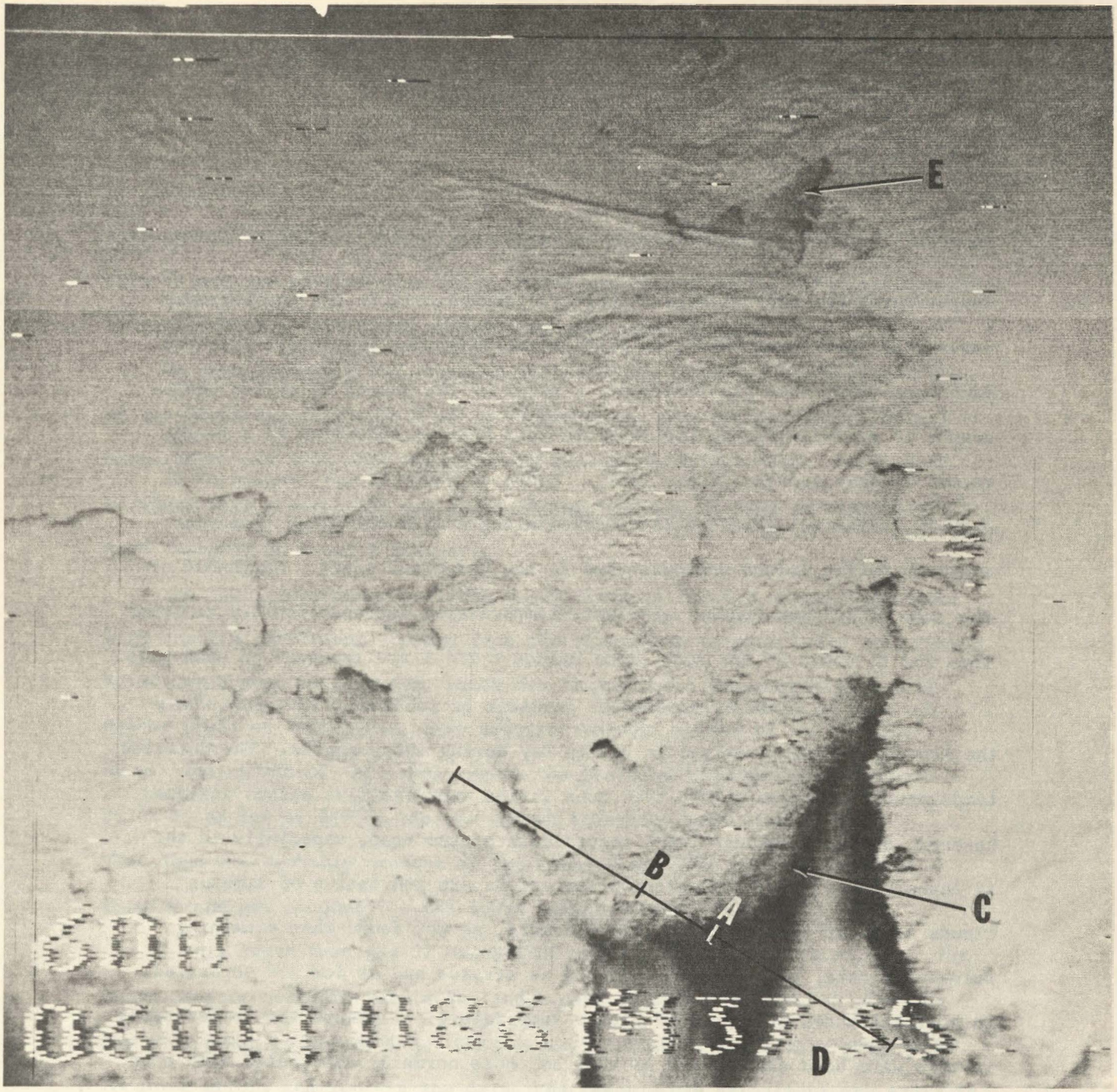

Figure 4-3 Nimbus-4 IDCS photograph showing Baffin Bay area, 27 March 1971. Location of data swath shown in Figure 4-4 is indicated. The ice edge is at C with stratus cloud (D) to the south. Cloud bands cross northern Baffin Bay just south of the "North Open Water" area, which is at E.

temperatures are several degrees higher, particularly in the two February cases (the North Open Water, or North Water Polynyna, is characterized by much open water even in mid-winter; a study of the use of satellite photographs to evaluate spring ice cover in this area is described in a recent report by Aber and Vowinckel, 1971). South of Davis Strait, except on 12 January, a thermal gradient is observed along a line extending from near southern Baffin Island northeastward to the Greenland coast. Northwest of the zone of maximum thermal gradient, temperatures decrease rapidly to lower than 264°K; south of the zone, some values $\geq$ 274°K are recorded on each pass.

The zone of maximum temperature gradient is located in the area where the ice edge normally exists in Baffin Bay during these months. The detailed temperature structure within this zone varies over the five passes analyzed, however, and many values <274°K occur south of the zone, especially in the 12 January map. These temperature variations are indicative of stratus clouds south of the ice cover. Furthermore, as was found when examining film-strip data, the areas interpreted as stratus and as ice are separated in most instances by a band of higher temperature. Although the temperatures in this warm band are not all as high as those normally associated with open water, they are higher than the values measured over the ice to the north and over the stratus to the south; thus, the narrow band probably contains broken stratus cloud with more solid cloud cover to the south.

Although not shown on the map, the IR measurements over the land areas are generally lower than those measured over Baffin Bay. In northern parts of the Bay, however, a thermal gradient between the pack ice and the land cannot always be distinguished. On 9 January, for example, the Smith Sound

area cannot be mapped, and a large range of temperatures is observed (although most values are greater than 252°K, a few are in the 240's). At least on this date, therefore, some cloud probably existed over the area.

As seen in Figure 4-2, compact ice cover was reported along almost the entire Birds-Eye flight path on 11-12 February. One observation of only 3 oktas cover was made near the northern end of the flight path; just north of where this observation was made, IR temperatures as high as 272° to 274°K were measured on 5 and 7 February.

The ITOS temperature analysis on 27 March is in good overall agreement with the ice conditions deduced from the photograph (Figure 4-3). The "North Water" area near Smith Sound, which has temperatures somewhat higher than nearby areas of Baffin Bay, also appears somewhat darker in the visible data. Just south of this area, where the measured temperatures are from 252°K to as low as 240°K, the photograph indicates some cloud-cover. The cloud was probably present at the time of the ITOS pass a few hours earlier and may account for the lower temperatures.

A data swath from the 27 March ITOS pass is plotted in Figure 4-4. The swath crosses southern Baffin Bay and a part of Baffin Island, as shown on the photograph in Figure 4-3. Considering that there are slight geographic location errors inherent in the data, the temperature variations are again in good agreement with the ice concentrations deduced from the photograph. Between points A and B, where the temperature varies considerably, the photograph shows variations in brightness which likely are associated with varying ice concentrations. The stratus cloud seen in the photograph south of the principal ice edge displays IR temperatures somewhat higher than the ice but lower than the open water.

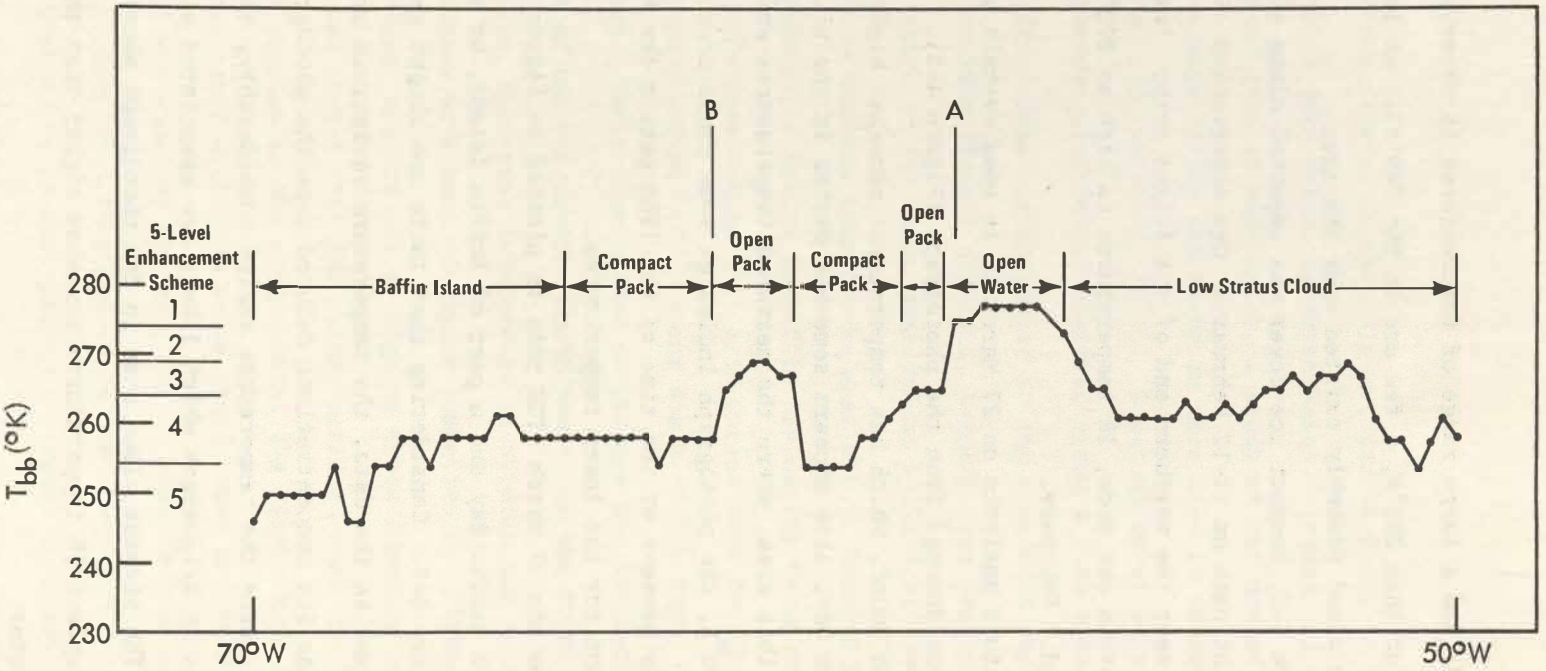

Figure 4-4 Data swath plotted from ITOS-1 SR digitized map, 27 March 1971. Location of swath is shown in Figure 4-3.

4.2 Analysis of Temperatures for Selected Areas of Baffin Bay

In addition to the analysis using the 5-level mapping scheme, temperature frequency distributions and mean temperatures were computed for 26 cells within Baffin Bay (each of 1^{o}-latitude by 5^{o}-longitude), one cell in Smith Sound, and two cells over the Greenland ice cap. In most instances, 9 to 16 data points near the center of the cell were used; in northernmost Baffin Bay a larger number of data points were used in order to cover most of Smith Sound. The locations of the cells are shown in Figure 4-5, and the mean temperatures for the five dates analyzed are given in Table 4-2.

The mean overall temperature values for all of the Baffin Bay cells are consistent for the two January passes (three days apart). On a cell-to-cell basis, the February data are very consistent, with the greatest temperature difference for any cell being only 4°K. Overall, the mean value is the highest for the February data and the lowest for the March data. For the two Greenland cells, the mean value is also the lowest for the March case; for this area, however, the highest values are in January rather than February.

The mean temperatures for individual cells over the five dates are between 249° and 254°K, except for the southernmost cells. Thirteen of the 26 cells have mean values of 250° or 251°K. The lowest single value is 243°K for cell No. 13 on 12 January, and the highest is 271°K for cell No. 26 on 9 January. The range in values is greater for the northernmost and southernmost cells. The data points of the southernmost cells are in the area of the ice boundary where conditions can vary between ice, water, or even stratus cloud. In the north, some of the data points are near Smith Sound, which contains the North Open Water area discussed in the previous section. In fact, the cell within Smith Sound is seen to be consistently warmer than the Baffin Bay cells, except on 9 January when cloud apparently covers the area.

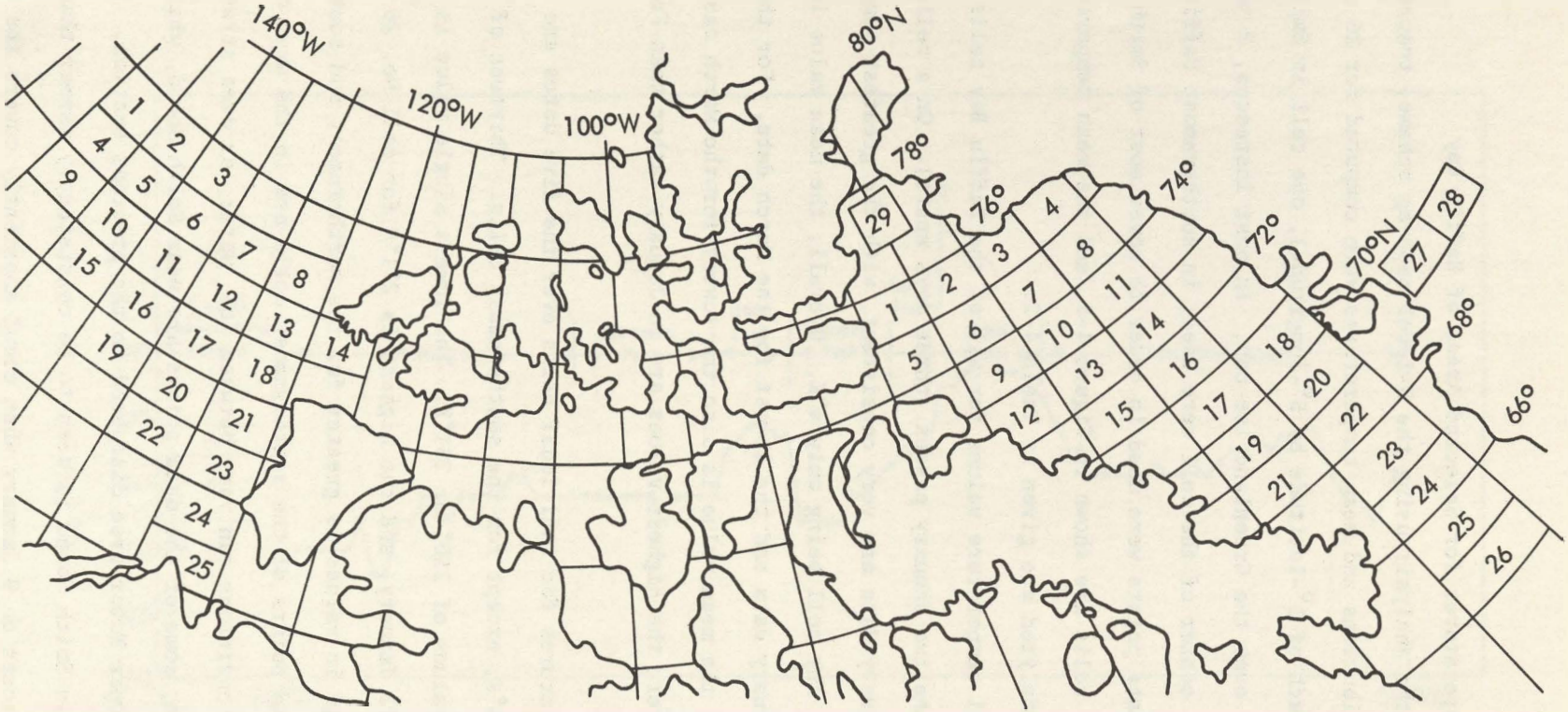

Figure 4-5 Location of cells in Baffin Bay and Beaufort Sea areas used in analysis of ITOS and Nimbus temperatures.

TABLE 4-2

ITOS-SR TEMPERATURES FOR CELLS IN BAFFIN BAY AREA

Baffin Bay Cell No.	Temperature (°K) 9 Jan	12 Jan	5 Feb	7 Feb	27 Mar	Mean	Range
1	250	251	261	261	249	254	12
2	250	244	260	257	246	251	16
3	250	251	256	258	245	252	13
4	252	251	253	251	244	250	9
5	251	246	254	254	245	250	9
6	252	243	257	253	246	250	11
7	249	250	255	252	245	250	10
8	255	252	253	253	245	252	10
9	253	249	254	255	246	251	10
10	256	249	253	254	245	251	11
11	250	252	251	254	247	251	7
12	253	250	253	250	246	250	7
13	251	243	253	251	245	249	10
14	245	251	253	253	247	250	8
15	252	249	253	252	248	251	5
16	250	252	254	251	247	251	7
17	247	253	254	257	248	252	7
18	251	258	253	250	255	253	8
19	253	253	249	248	250	251	5
20	254	254	252	254	253	253	2
21	251	252	253	255	251	252	4
22	257	257	255	257	258	257	3
23	258	251	260	259	260	258	9
24	258	253	265	261	261	260	12
25	263	257	265	265	263	263	8
26	271	256	265	268	264	265	15

contd.

TABLE 4-2 CONTINUED

	Temperature (^{o}K)					
	9 Jan	12 Jan	5 Feb	7 Feb	27 Mar	Mean
Mean for 26 Baffin Bay Cells	253	251	256	255	250	-
Range of Values for 26 Baffin Bay Cells	245-271	243-258	249-265	248-268	244-264	-
Smith Sound (Cell 29)	251	257	263	262	253	257
Difference Between Baffin Bay Mean Value and Smith Sound	-2	6	7	7	3	4
Greenland (Cell 27)	255	258	254	251	243	252
Greenland (Cell 28)	248	246	240	238	231	241
Greenland (Mean)	252	252	247	245	237	-

- Location of Cells are given in Figure 4-5

- Temperature Value for each cell is the mean of 16 or more data points centered in cell.

The difference is also smaller on 27 March, indicating that some cloud obscuration may be affecting the measurements on this date, as well; the photograph (Fig. 4-3) shows that some cloud cover over Smith Sound is quite possible.

Examination of the individual cell temperatures reveals that in 14 of the 26 Baffin Bay cells, the lowest value is on 27 March. As a further check of the magnitude of the difference between the February and March measurements, temperature frequency distributions were compiled for all data points in the Greenland cells (about 130) and in the Smith Sound cell (about 90). For the two Greenland cells, the maximum frequencies in the 5 February data are 248 to 252°K and 240 to 244°K; in March the maximum frequencies for the respective cells are 240 to 244°K and 228 to 232°K, nearly 10°K lower. In Smith Sound, the 5 February distribution is relatively flat with the maximum frequency occurring at 266 to 268°K; on 27 March, the distribution has a pronounced peak at 252 to 256°K, more than 10°K lower. (as discussed in the previous paragraph, however, some cloud obscuration may exist over Smith Sound on 27 March).

Meteorological data for stations on the coast of Greenland and on Baffin Island show that temperatures near the time of satellite passage are actually somewhat higher on 27 March than on 5 February. The lowest reported on the March date is 244°K and on the February date 239°K. All stations on these two dates as well as on 7 February and 12 January report clear skies or only scattered cloud (one station on the coast of Greenland reports overcast on 5 February). On 9 January, the date on which the IR measurements indicate some cloud obscuration, most stations do report overcast conditions. The lowest temperatures reported on both 9 and 12 January are also of the order of 244°K.

In the arctic region for which the maps were analyzed, it is difficult to obtain a reliable calibration of the data because the measurements were made almost entirely over land or ice-covered water where surface temperatures can vary considerably. In order to gain some idea of the range of temperatures measured over a relatively stable feature, the maximum values mapped in areas south of Davis Strait were examined. During the winter season, oceanic areas in which temperatures are greater than 273°K are presumably both ice-free and free of stratus cloud (from the scant meteorological data available, it appears that surface temperatures over the area examined are well below 273°K at the times of the January and February ITOS passes; on 27 March, the highest temperature reported is 273°K at a station in southern Greenland).

The maximum ITOS temperature values measured south of Davis Strait on each date of the sample are shown in Table 4-3. Because of the prevalence of stratus, the actual cloud-free locations varied somewhat from day to day; on four of the dates, however, temperatures exceeding 273°K were measured over approximately the same area (near 60°N, 58°W). In this area, the maximum IR temperatures on each of the ITOS maps are of the order of 280°K and do not vary greatly from month to month, although the March value is somewhat lower than the February values.

Table 4-3 also contains ship reports of sea surface temperatures measured near the location for which the ITOS measurements were made. The ship reports are consistently lower than the ITOS values, particularly in January and February. It is of interest, however, that Weather Ship 4YB reported a somewhat lower sea surface temperature in March than in February. Similarly, normal values for a grid point at 62.5°N, 56.5°W (available from the

TABLE 4-3

A. MAXIMUM ITOS-SR TEMPERATURES MEASURED SOUTH OF DAVIS STRAIT

Date (1971)	Location	Temperature (^{o}K)
9 January	Labrador Sea (59^{o}N, 58^{o}W)	278 $\leq$ T < 280
12 January	South of Greenland (58^{o}N, 45^{o}W)	288 $\leq$ T < 292
5 February	South of Greenland (58^{o}N, 45^{o}W)	292 $\leq$ T < 296
	Labrador Sea (56^{o}N, 58^{o}W)	280 $\leq$ T < 284
7 February	South of Greenland (58^{o}N, 45^{o}W)	288 $\leq$ T < 292
	Labrador Sea (61^{o}N, 58^{o}W)	280 $\leq$ T < 284
27 March	Labrador Sea (61^{o}N, 58^{o}W)	278 $\leq$ T < 280

B. REPORTED SEA SURFACE TEMPERATURES

Date (1971)	Location and Source		Temperature (^{o}K)
9 January	57^{o}N, 51^{o}W	Weather Ship 4YB	275-276
10 January	61^{o}N, 50^{o}W	Ship Report	273.5
12 January	57^{o}N, 51^{o}W	Weather Ship 4YB	275-276
	62^{o}N, 52^{o}W	Ship Report	275
5 February	57^{o}N, 51^{o}W	Weather Ship 4YB	275-276
6 February	63.5^{o}N, 53.5^{o}W	Ship Report	272.5
7 February	57^{o}N, 51^{o}W	Weather Ship 4YB	275-276
27 March	57^{o}N, 51^{o}W	Weather Ship 4YB	274-275
27 March -	61.5^{o}N, 56^{o}W	German Tss Collection	273.2
4 April	60^{o}N, 50^{o}W	German Tss Collection	275.6

Navy, FWC Monterey) also give a March temperature of 270.8°K compared with 272.1°K in February and 273.1°K in January. Thus, at least over the open water areas temperatures apparently do decrease from February to March.

The external correction provided by the ship reports indicates that the absolute temperatures measured by ITOS are 5°K or more too high, with the error being somewhat more pronounced in February. The error undoubtedly can be attributed to the Scanning Radiometer calibration problems discussed earlier in Section 2.2. The decrease in temperature from February to March observed in both the ship reports and ITOS data, however, does provide further evidence that the relative temperature values measured by ITOS are useful.

4.3 Comparison Between ITOS and Nimbus Data

For 9 and 12 January and 27 March, ITOS temperature measurements were compared with nearly concurrent Nimbus measurements. For the two January dates, mean temperatures were computed for selected cells in Baffin Bay and over the Greenland ice cap. The mean temperatures for the cells, each of which contained nine data points, are given in Table 4-4.

On both dates, the Nimbus values are lower than the ITOS. On 9 January, the difference is about 15°K, whereas on 12 January, the difference is as great as 37°K for one cell. Examination of the Nimbus grid-print map for the latter date revealed some temperature values as low as about 210°K. These values are much lower than any values measured by ITOS and are lower than any values found previously using Nimbus HRIR data. Although the 9 January temperatures are closer to those measured by ITOS, the values still appear to be somewhat too low. Because the Nimbus maps covered only the

TABLE 4-4

COMPARISON BETWEEN ITOS-SR AND NIMBUS THIR TEMPERATURES FOR SELECTED CELLS IN BAFFIN BAY AREA

Location of Cell	Temperature (^{o}K) 9 January ITOS	9 January Nimbus	9 January ITOS-Nimbus	12 January ITOS	12 January Nimbus	12 January ITOS-Nimbus
Baffin Bay						
74^{o}N, 65^{o}W	247	233	14	250	221	29
72^{o}N, 60W	247	234	13	255	218	37
Greenland						
74^{o}N, 50^{o}W	255	237	18	254	223	31
70^{o}N, 45^{o}W	255	231	24	243	213	30

- Temperature Values are for 9 Data Points Centered at Location Specified.

area north of about 70°N, it was not possible to check the Nimbus values with respect to an ice-free ocean area.

The January Nimbus data were, therefore, concluded to be of questionable value, and a more extensive comparison between Nimbus and ITOS measurements was limited to the 27 March data. On this date, in addition to passes by each satellite over Baffin Bay, data from passes over the Beaufort Sea were also acquired. Mean temperatures were computed for 20 cells in Baffin Bay and 25 cells in the Beaufort Sea. The locations of the cells are given in Figure 4-5 and the temperatures are given in Table 4-5. In these computations, all data points within each cell were used. For each cell, the ITOS maps contain 100 or more data points, whereas the Nimbus maps contain 20 to 40 points.

Table 4-5 shows that in 19 of the 25 Beaufort Sea cells and in all 20 Baffin Bay cells, the mean ITOS temperature is higher than the mean Nimbus temperature. The differences are consistent, the mean value being about 2.5°K for each area. In the Beaufort Sea, the maximum difference is 8°K in cell No. 2; of the cells in which the Nimbus value exceeds the ITOS, the maximum difference is 4°K, in cell Nos. 8 and 25. In Baffin Bay, the maximum difference is 5°K in cell No. 18.

For the 27 March passes corresponding ITOS and Nimbus data swaths across Smith Sound and Banks Island were plotted. The swaths are shown in Figure 4-6 (a and b). In the data for Smith Sound (the North Water Polynya area) the agreement between the ITOS and Nimbus values is good. In the swaths from the other passes, the agreement is also good for the portions of the swaths over the Beaufort Sea. Near the coast of Banks Island, however, a decrease in temperature measured by ITOS is not observed in the

TABLE 4-5
ITOS-SR AND NIMBUS THIR TEMPERATURES FOR BEAUFORT SEA AND BAFFIN BAY CELLS, 27 MARCH 1971

Beaufort Sea				Baffin Bay			
	Temperature (^{o}K)				Temperature (^{o}K)		
Cell Number	ITOS	Nimbus	ITOS-Nimbus	Cell Number	ITOS	Nimbus	ITOS-Nimbus
1	249	243	6	1	249	246	3
2	249	242	7	2	246	243	3
3	247	244	3	3	245	243	2
4	249	244	5	4	244	241	3
5	249	243	6	5	245	244	1
6	247	244	3	6	246	243	3
7	243	246	-3	7	245	243	2
8	241	245	-4	8	245	242	3
9	247	243	4	9	246	244	2
10	247	243	4	10	245	243	2
11	247	243	4	11	247	243	4
12	243	243	0	12	246	242	4
13	243	243	0	13	245	244	1
14	242	243	-1	14	247	243	4
15	245	241	4	15	248	247	1
16	247	241	6	16	247	245	2
17	243	240	3	17	248	246	2
18	245	242	3	18	255	250	5
19	244	241	3	19	250	247	3
20	243	239	4	20	253	250	3
21	244	243	1				
22	242	241	1		Mean Difference		2.7
23	243	241	2				
24	241	242	-1				
25	235	234	1				
	Mean Difference		2.4				

Location of Cells are given in Figure 4-5. Temperature Value for each cell is the mean of all data points within that cell (about 100 points for ITOS; 40 for Nimbus).

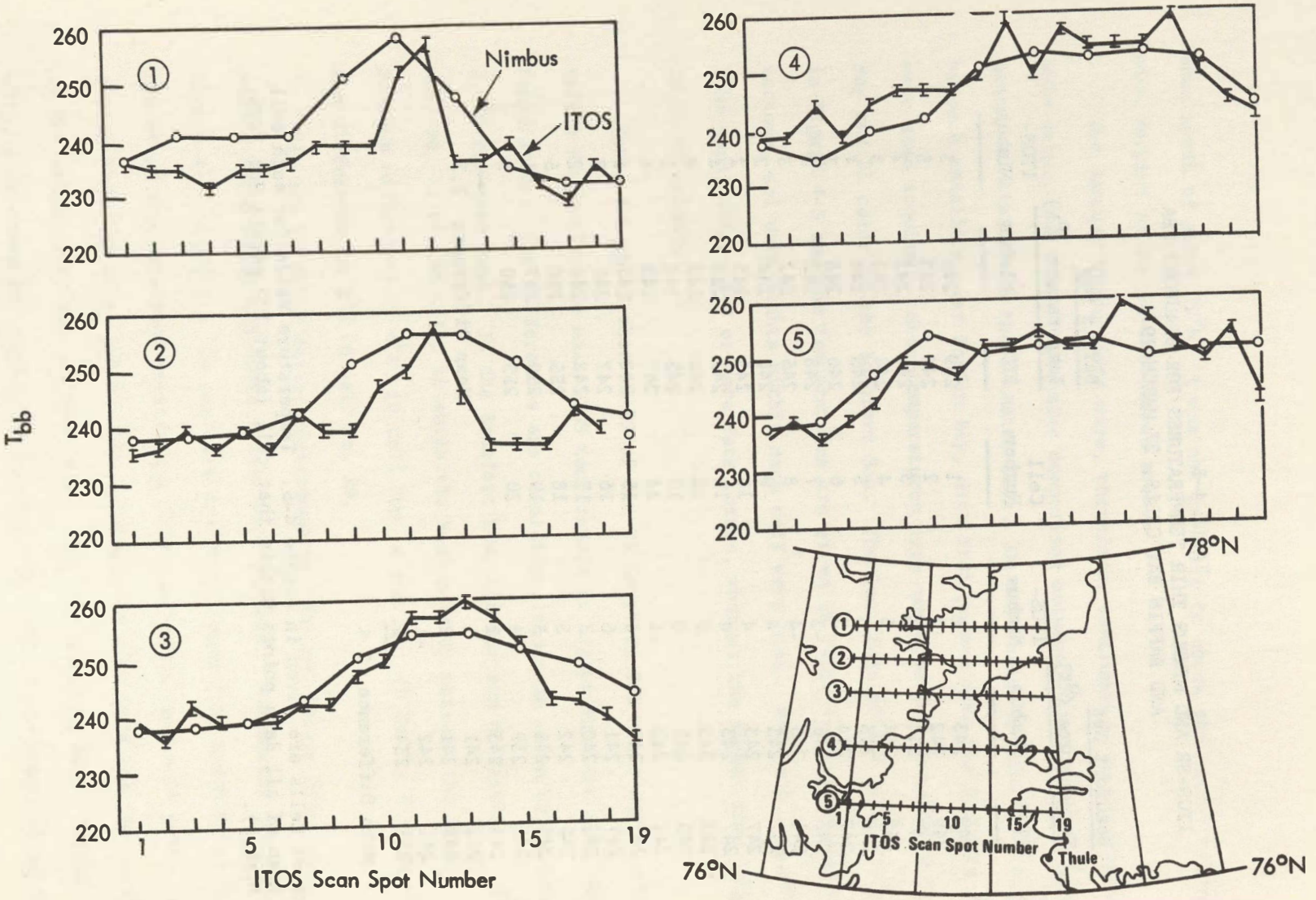

Figure 4-6a Comparison between ITOS-1 and Nimbus-4 data swaths crossing Smith Sound-Kane Basin area, 27 March 1971.

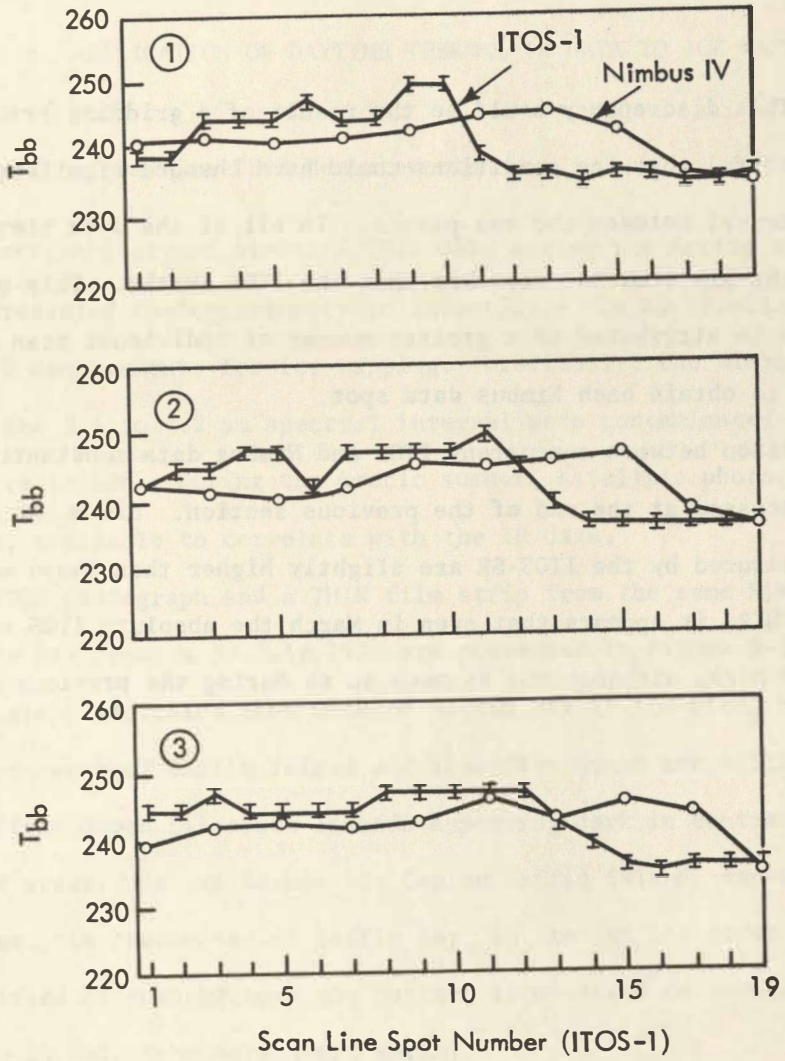

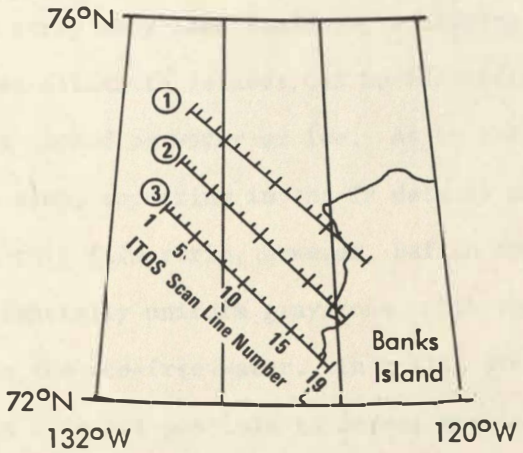

Figure 4-6b Comparison between ITOS-1 and Nimbus-4 data swaths near Banks Island, 27 March 1971.

Nimbus data. This discrepancy could be the result of a gridding error, since it is doubtful that ice conditions could have changed significantly in the time interval between the two passes. In all of the data plotted, the Nimbus swaths are somewhat smoother than the ITOS swaths. This effect can most likely be attributed to a greater number of individual scan spots being averaged to obtain each Nimbus data spot.

The comparison between concurrent ITOS and Nimbus data substantiates the results discussed at the end of the previous section. Since the overall temperatures measured by the ITOS-SR are slightly higher than those measured by the Nimbus THIR, it appears that even in March the absolute ITOS values are erroneously high, although not as much so as during the previous month.

5. APPLICATION OF DAYTIME THERMAL IR DATA TO ICE MAPPING

5.1 Analysis of Daytime THIR Measurements

The availability of Nimbus-4 THIR data during the Arctic summer season of 1970 presented the opportunity to investigate the application of daytime thermal IR measurements for ice mapping. Previously, the Nimbus HRIR measurements in the 3.4 to 4.2 μm spectral interval were contaminated during daytime by solar radiation. During the Arctic summer, satellite photography is, of course, available to correlate with the IR data.

An IDCS photograph and a THIR film strip from the same Nimbus pass over the Baffin Bay area on 30 July 1970 are presented in Figure 5-1 (a and b). The photograph indicates that much of Baffin Bay is ice-free, but that most water areas west of Baffin Island and Lancaster Sound are still ice covered, the snow-free Queen Elizabeth Islands appearing dark in contrast. Various glaciated areas, such as Barnes Ice Cap on Baffin Island, can be easily identified. In the center of Baffin Bay, an area of ice cover exists; this is identified as such because the pattern is observed on several other days, including 29 July (photograph not shown).

In the THIR film strip many land features, including the coastal area of Greenland and the Queen Elizabeth Islands, can be identified because they appear warmer than the surrounding water or ice. As in the photograph, the Barnes Ice Cap can be seen, appearing in the IR data as an area colder than its surroundings. In this film strip, however, Baffin Bay and other water areas appear in an essentially uniform gray tone, with the ice cover being indistinguishable from the ice-free water. In a film strip on the previous day (not shown), it is also not possible to detect the ice. In the 30 July film strip, a cloud obscures a part of Baffin Bay and the Greenland coast;

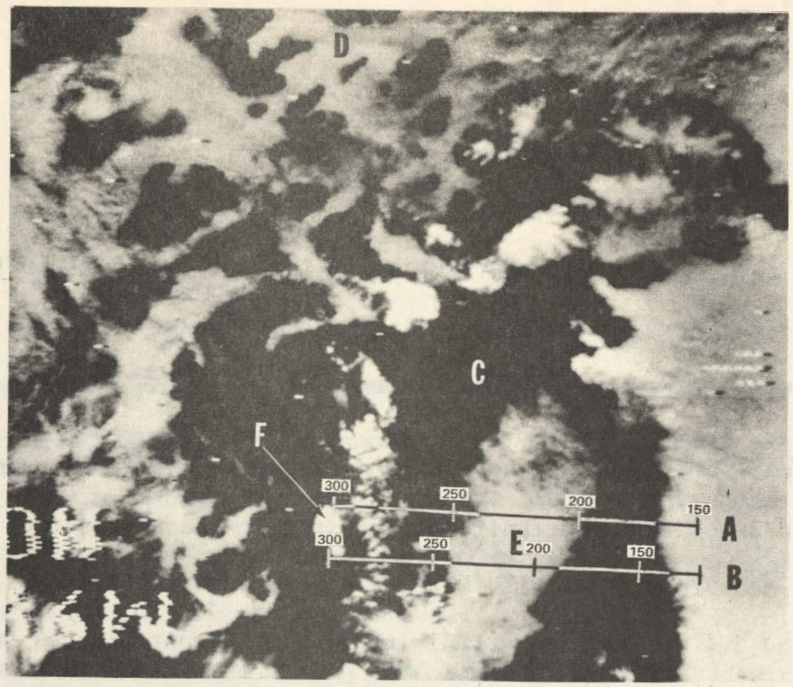

(a) IDCS Photograph

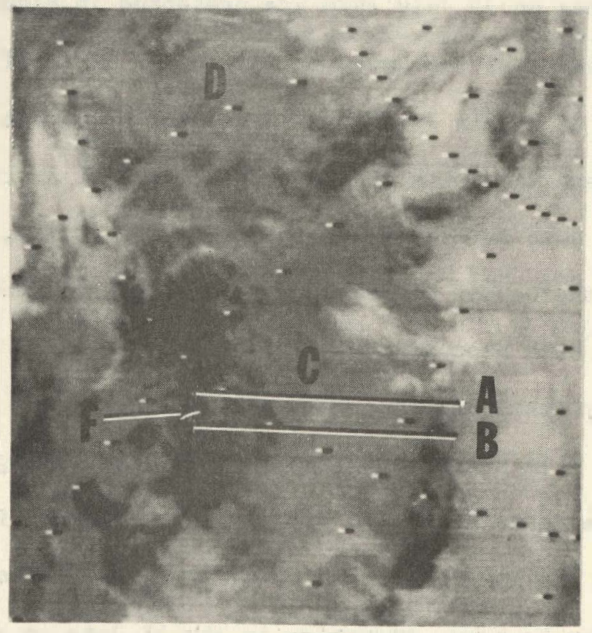

(b) Daytime THIR Film Strip

Figure 5-1 Nimbus-4 IDCS photograph and concurrent THIR film strip showing area from Baffin Bay (C) to Queen Elizabeth Islands (D), 30 July 1970. Locations of the scan lines plotted in Figure 5-2 are indicated at A and B. Ice in Baffin Bay (E) visible in the photograph cannot be detected in the film strip. Barnes Ice Cap is at F.

since the cloud is nearly transparent in the photograph, it is presumably thin cirrus that is radiating enough energy to be detectable in the thermal IR measurement.

From full-resolution digitized data listings for this same Nimbus orbital pass, several scan lines crossing from Greenland to the Barnes Ice Cap on Baffin Island were plotted. Two of the scan lines, located as shown in Figure 5-1 (a and b), are given in Figure 5-2. The scan lines demonstrate that the temperatures measured over the Baffin Bay ice are, in reality, somewhat lower than those measured over the water. However, although the values are about what would be expected for ice, no well-defined temperature gradient separates the ice from the water. Furthermore, the small temperature difference cannot be detected in the film strip because the entire range of temperature measured over the ice and water falls into the same gray-scale level (see scale on right side of Figure 5-2).

A Nimbus daytime THIR film strip and concurrent IDCS photograph from a pass crossing the eastern Beaufort Sea on 17 July are presented in Figure 5-3 (a, b). In the photograph, M'Clure and Prince of Wales straits, to the north and east of Banks Island, are readily seen to be ice filled since the snow-free islands appear dark in contrast. A narrow band of ice also exists along the west coast of Banks Island, the edge of the Beaufort Sea ice pack being located a little farther west. As was true in the Baffin Bay data, land features appear distinctly warmer than their surroundings in the thermal IR film strip. Again, however, the entire water area appears at the same temperature range (uniform gray tone), regardless of ice distribution. Clouds, at least those that are colder than the ice, are more easily distinguished from the ice in the IR imagery than they are in the IDCS photograph.

A scan-line analysis from the data listings for the same pass is shown in Figure 5-4 (the locations of the four scan lines are indicated in Figure 5-3). In this analysis the land areas are very warm, having temperatures

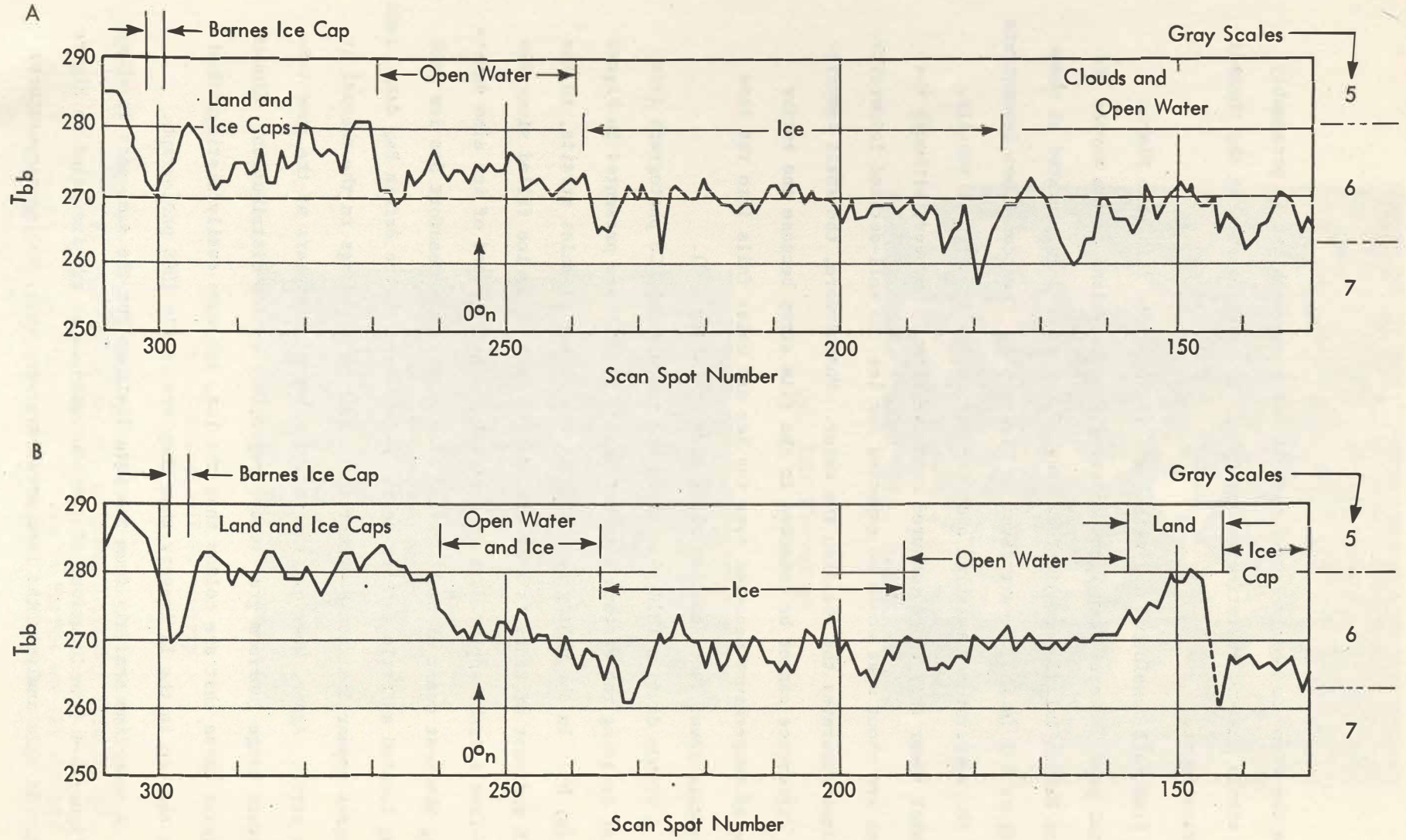

Figure 5-2 Analysis of digitized temperature values for scan lines shown in Figure 5-1; Nimbus-4 THIR, 30 July 1971.

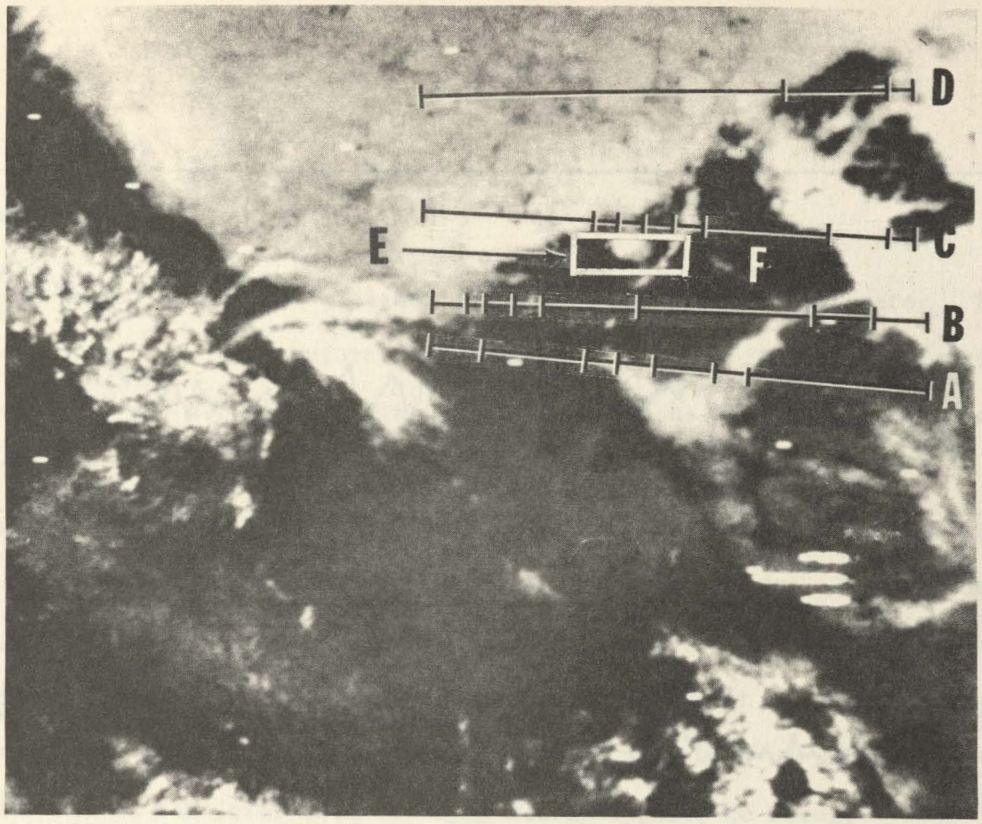

(a) IDCS Photograph

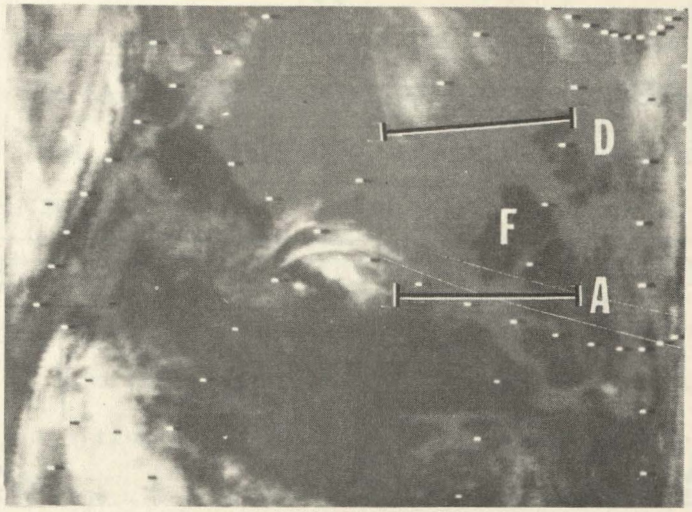

(b) Daytime THIR film strip

Figure 5-3 Nimbus-4 IDCS photograph and concurrent THIR film strip showing Banks Island and eastern Beaufort Sea area, 17 July 1970. Scan lines plotted in Figure 5-4 are indicated at A through D. Area analyzed in Figure 5-5 is indicated at E. Banks Island is at F; ice visible in photograph cannot be detected in film strip.

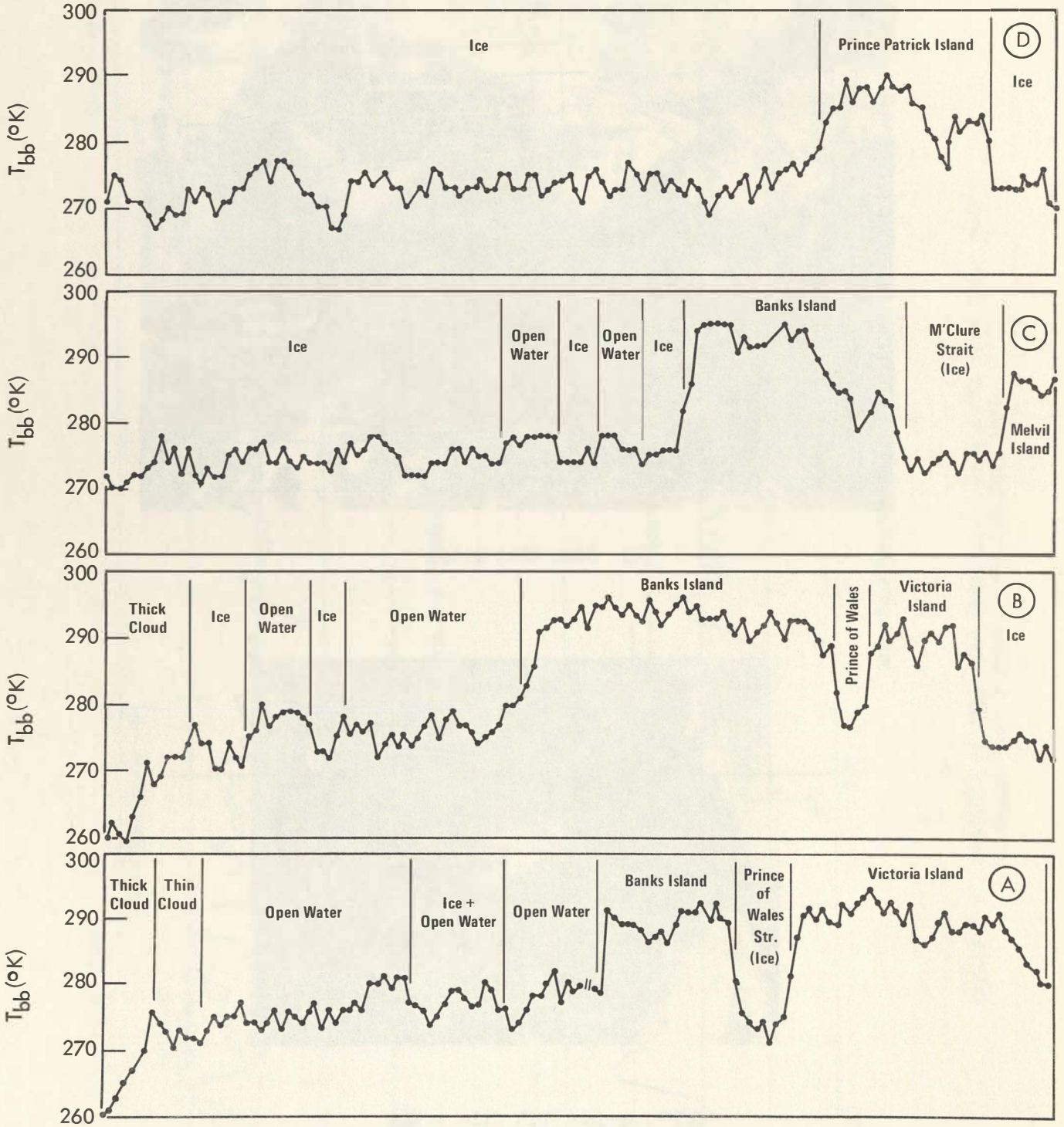

Figure 5-4 Analysis of digitized temperature values for scan lines shown in Figure 5-3; Nimbus-4 THIR, 17 July 1970.

as high as 295°K, some 20°K higher than the surrounding ice or water. The measurements over the Beaufort Sea and the two straits fluctuate primarily between 272° and 273°K; the highest values are about 280°K, and a few scan spots are as low as 270°K. Although the temperature does fluctuate and the values are somewhat higher than would be anticipated, there is some indication of a correlation between the temperature and ice cover. The values along Scan-line D, which is almost completely over ice, are consistently lower than the values along the scan lines farther south, which cross open water. Also, in Scan-line C, the measurements just west of Banks Island are as much as 5°K lower when crossing ice as opposed to water.

In the IDCS photograph, what appears to be an isolated ice floe is observed west of Banks Island (Area E in Figure 5-3a). A temperature analysis derived from nine contiguous scan lines across this area is shown in Figure 5-5. Again, although the measured values are consistently equal to or greater than 273°K, the ice floe can be detected; most of the values over the floe are lower than 276°K, whereas the values over the open water are mostly between 276° and 280°K.

Another Nimbus daytime film strip and concurrent photograph crossing the same area on 29 June are shown in Figure 5-6 (a and b). Note that in this instance, a cloud crossing Banks Island is distinguishable in both the IR and visible data; thus, although the cloud has an effective temperature similar to that of the cloud observed in the Baffin Bay data discussed above, it must actually be a thicker cloud because of its higher reflectance.

Again, the water and ice areas appear in an essentially uniform gray level in the IR data. As in the previous case, scan lines were plotted to determine the temperature gradient across the water-ice boundary. In particular, an effort was made to see whether the apparently thicker ice floes

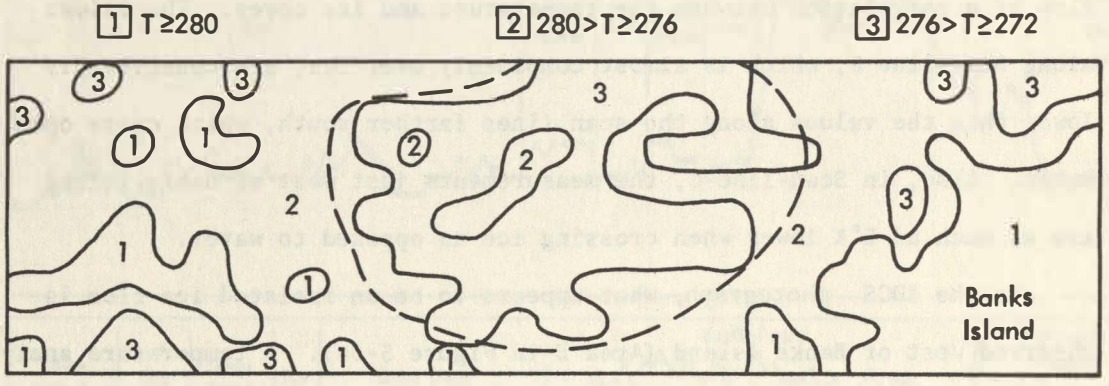

Figure 5-5 Analysis of digitized temperature values for area shown in Figure 5-3. Location of large ice floe seen in photograph (Fig. 5-3a) is indicated by broken line. Nimbus-4 THIR, 17 July 1970.

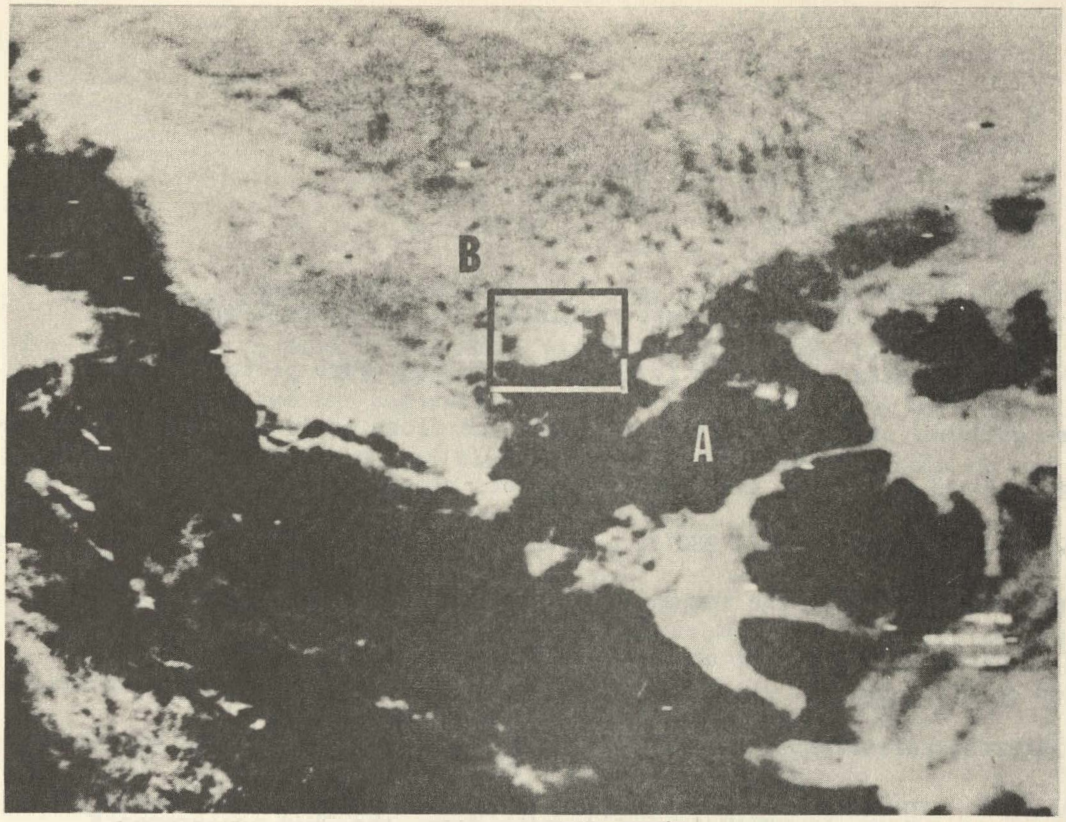

(a) IDCS Photograph

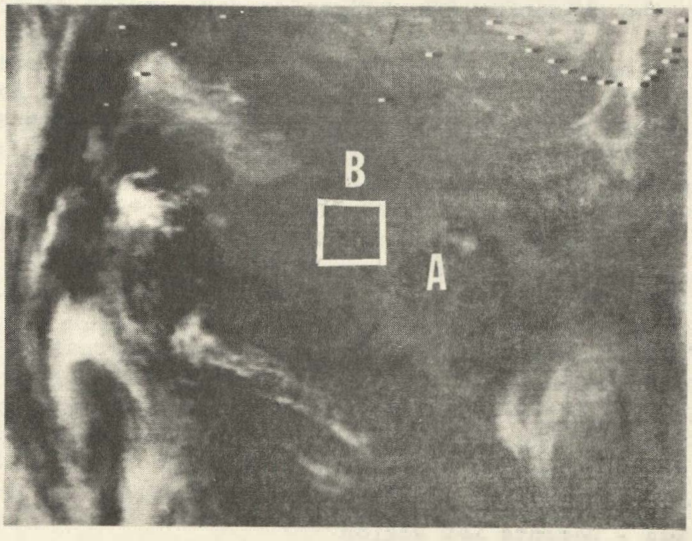

(b) Daytime THIR film strip

Figure 5-6 Nimbus-4 IDCS photograph and concurrent THIR film strip showing Banks Island (A) and eastern Beaufort Sea area, 29 June 1970. Specific area analyzed is shown at B. Ice floes within Area B visible in photograph are not detectable in film strip.

west of Banks Island (bright areas within area A in Figure 5-6a) are detectable in the IR data. Although full-resolution data were plotted for the entire outlined area, no indication of the ice floes could be found. Approximately two-thirds of the some 1000 scan spots plotted are greater than 274°K; a few values are as high as 280°K, and the minimum values are 267°K. Throughout the area, however, the temperatures appear to be randomly distributed, with no detectable gradient at the edge of the ice.

5.2 Diurnal Variations in Surface Temperature

Because of the availability of daytime data, the THIR measurements could also be used to examine the magnitude of the diurnal difference in surface temperatures for various ice features. The purpose of this investigation was to determine the feasibility of using these differences as an additional key for the objective identification and mapping of ice features. Two cases were selected for detailed analysis. In the first case, analysis was made of the digital data obtained over the Barents and Kara seas area of the USSR during both the daytime and nighttime passes (passes 133D and 142N) on 18 April 1970. The second case makes use of similar data obtained on 19 April 1970 (passes 151D and 147N) over the Baffin Bay area. For these dates the regions under investigation did experience alternating periods of sunshine and darkness. At 65-70^{o}N, approximately 15 hours of daylight exists during mid-April and the maximum solar elevation is about 30^{o} (List, 1966).

5.2.1 Kara Sea - Barents Sea Region

On 18 April 1970, the area over Novaya Zemlya and the adjacent seas of the USSR had essentially clear-sky conditions. These conditions are depicted in the IDCS photograph taken on the daylight pass over this region, shown in Figure 5-7. The concurrent THIR film-strip over the same area is

shown in Figure 5-8a. Also shown, as Figure 5-8b, is the THIR film-strip for the nighttime pass on the same date (pass 142). The locations of scan lines selected for analysis are shown in Figure 5-7. A more detailed depiction of the locations of these lines and their relationship to the geography and ice features deduced from the IDCS photograph is shown in Figure 5-9.

The digitized data used in the analysis were taken from full-resolution listings. Since the orientations of the lines shown in Figure 5-9 do not correspond to scan lines of the nighttime pass, the densities of data points along the analyzed lines for the two passes are quite different. This is evident in the analysis shown in Figure 5-10, in which the effective black-body temperatures for the daylight and nighttime pass along the indicated lines and are plotted separately. Also shown are longitudinal and latitudinal reference points as well as geographical and geophysical features deduced from the IDCS photograph.

The data in these graphs show,in general, that the daytime temperatures are higher than the corresponding nighttime temperatures. More significantly, the magnitude of the diurnal temperature difference, $\Delta T_{bb} = T_{bb}(\text{day}) - T_{bb}(\text{night})$, is dependent on the geophysical feature. Because of the difficulties in precise alignment of data points, it was not possible to obtain meaningful point-by-point values of ΔT_{bb}. Instead, mean values of T_{bb} (day) and T_{bb} (night) were computed for each significant segment of the data lines, corresponding to the mean T_{bb} values of the geophysical feature identified. From these mean values, representative values of ΔT_{bb} were computed. Results of these calculations for the data points over the Kara Sea and Barents Sea are shown in Table 5-1.

Figure 5-7 Nimbus-4 IDCS photograph showing Kara and Barents Seas area, 18 April 1970. Lines overlaid on photograph indicate the locations of contiguous THIR data points analyzed from Daytime and Nighttime Nimbus passes on same data. Ice concentrations interpreted from photograph are shown on map in Figure 5-9; THIR data points are plotted in Figure 5-10. Novaya Zemlya is at G, Coast of USSR at H.

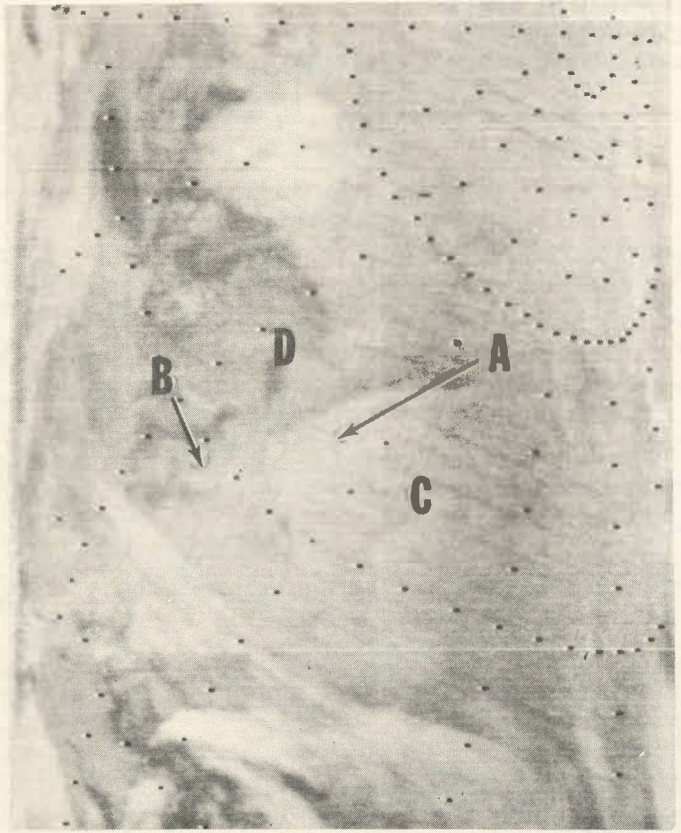

(a) Daytime THIR (Pass 133)

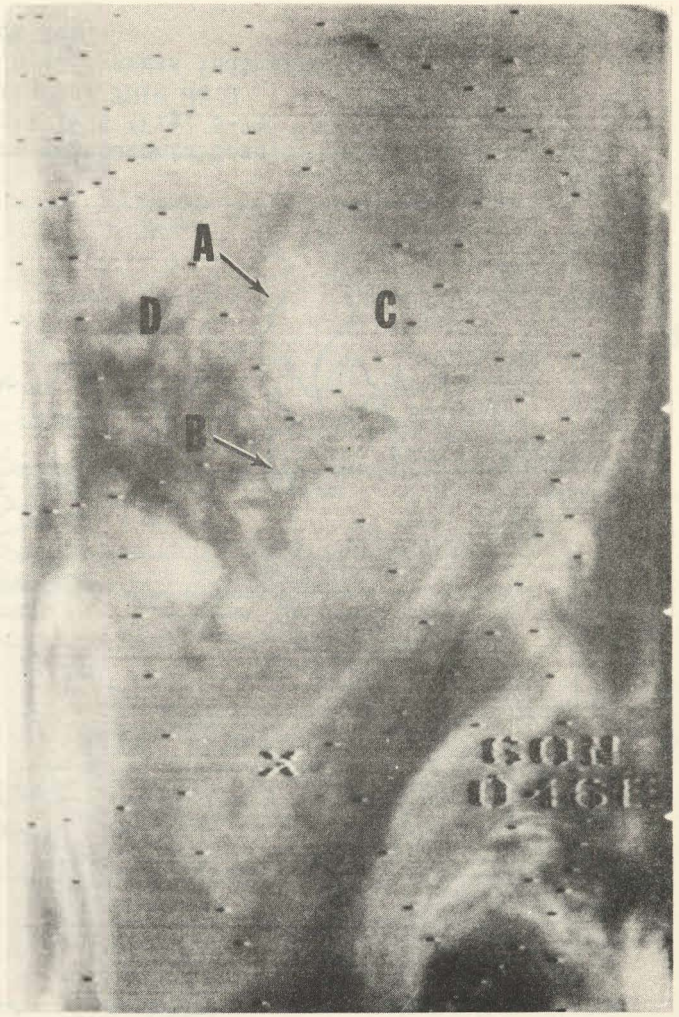

(b) Nighttime THIR (Pass 142)

Figure 5-8 Nimbus-4 Daytime and Nighttime THIR film strips showing Kara and Barents Seas area, 18 April 1970. Identifiable features include Novaya Zemlya (A), Ostrov Island (B), Kara Sea (C), and Barents Sea (D).

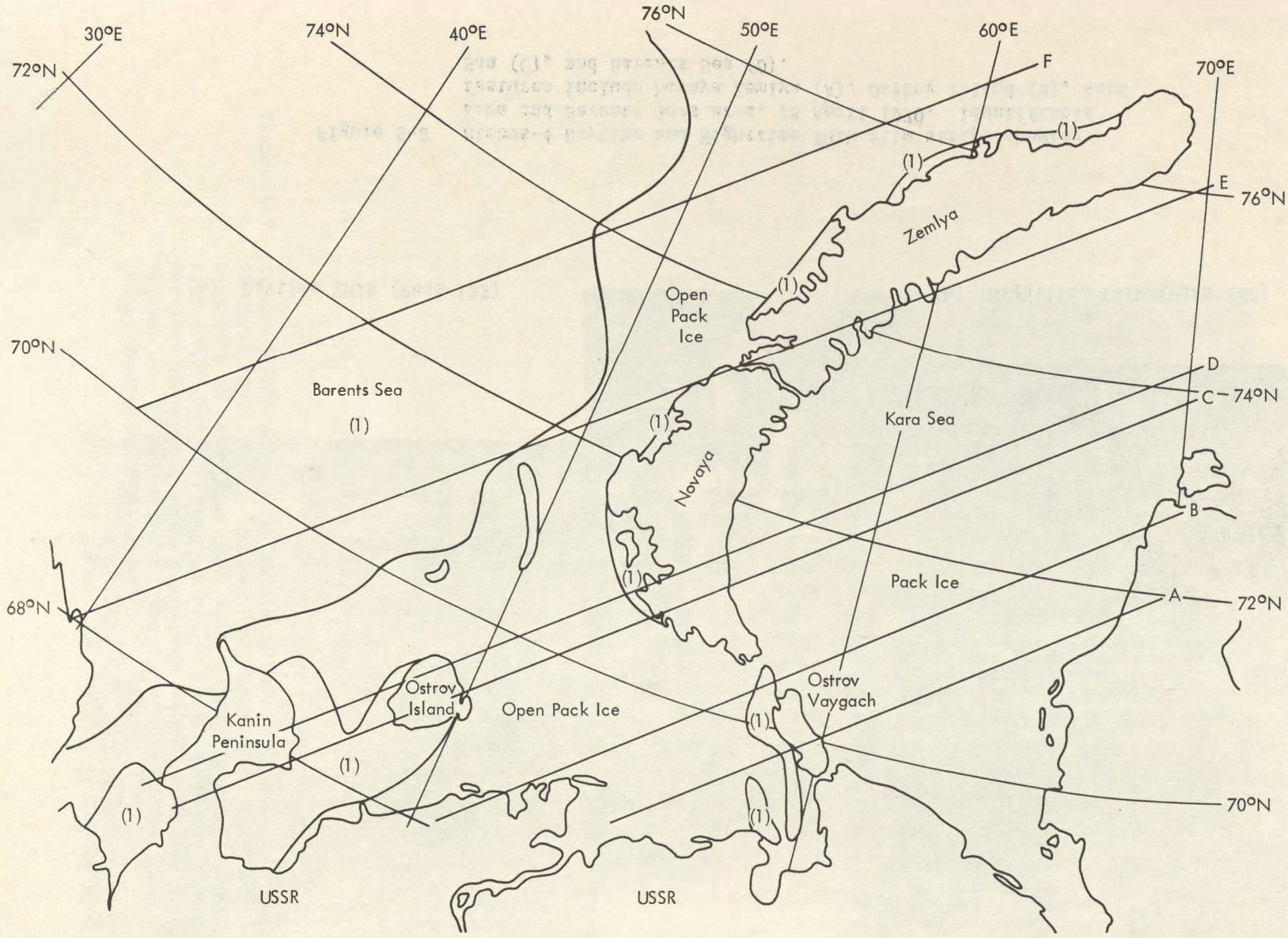

Figure 5-9 Map showing ice concentration in Kara and Barents Seas, derived from IDCS photograph, 18 April 1970 (Fig. 5-7). Lines indicate the locations of contiguous THIR data points, which are plotted in Figure 5-10. Areas indicated by (1) are Ice Free or Very Open Pack Ice.

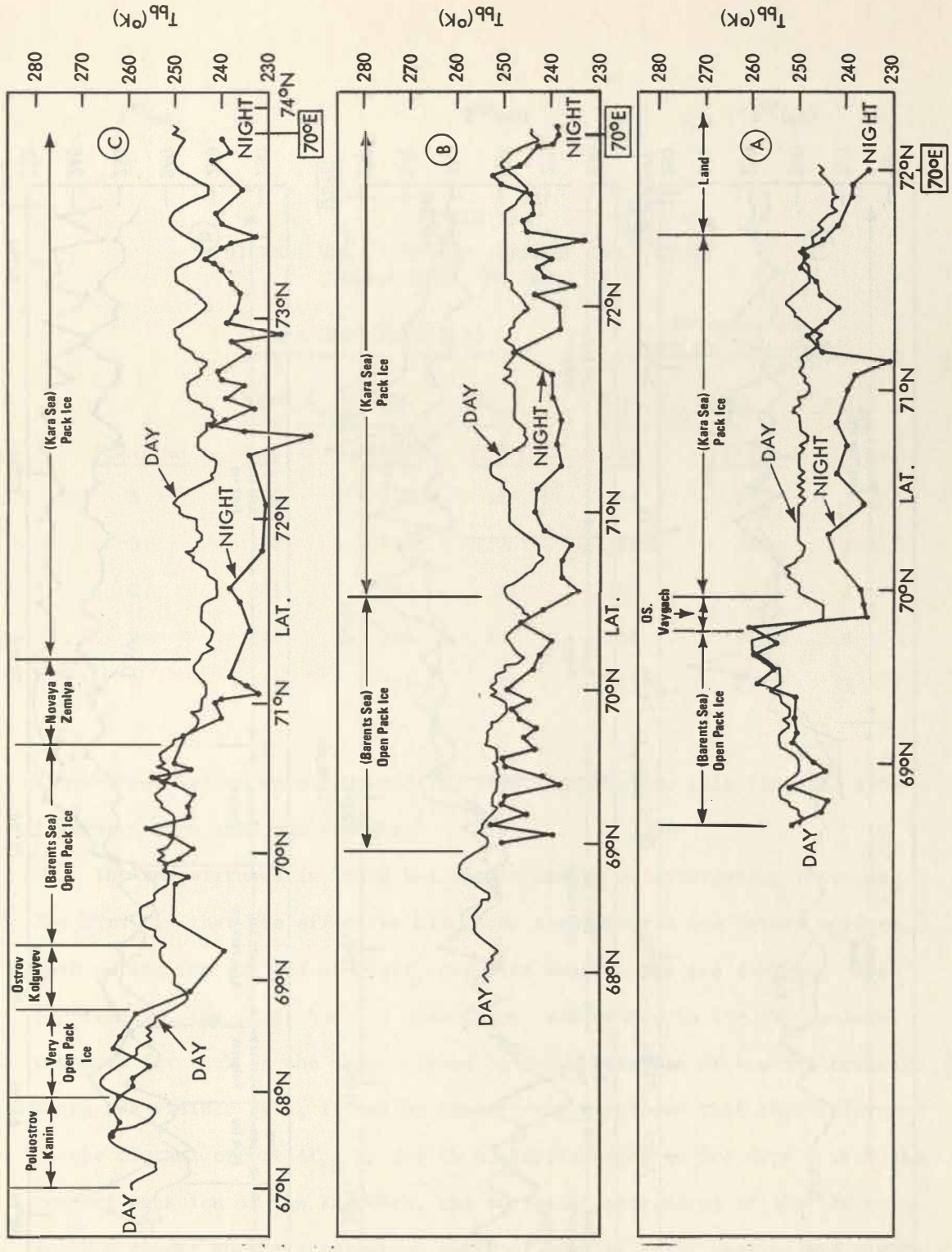

Figure 5-10. Digitized temperature values plotted for contiguous data points from Nimbus-4 Daytime and Nighttime passes on 18 April 1970. The location of the lines of contiguous data points are shown in Figures 5-7 and 5-9.

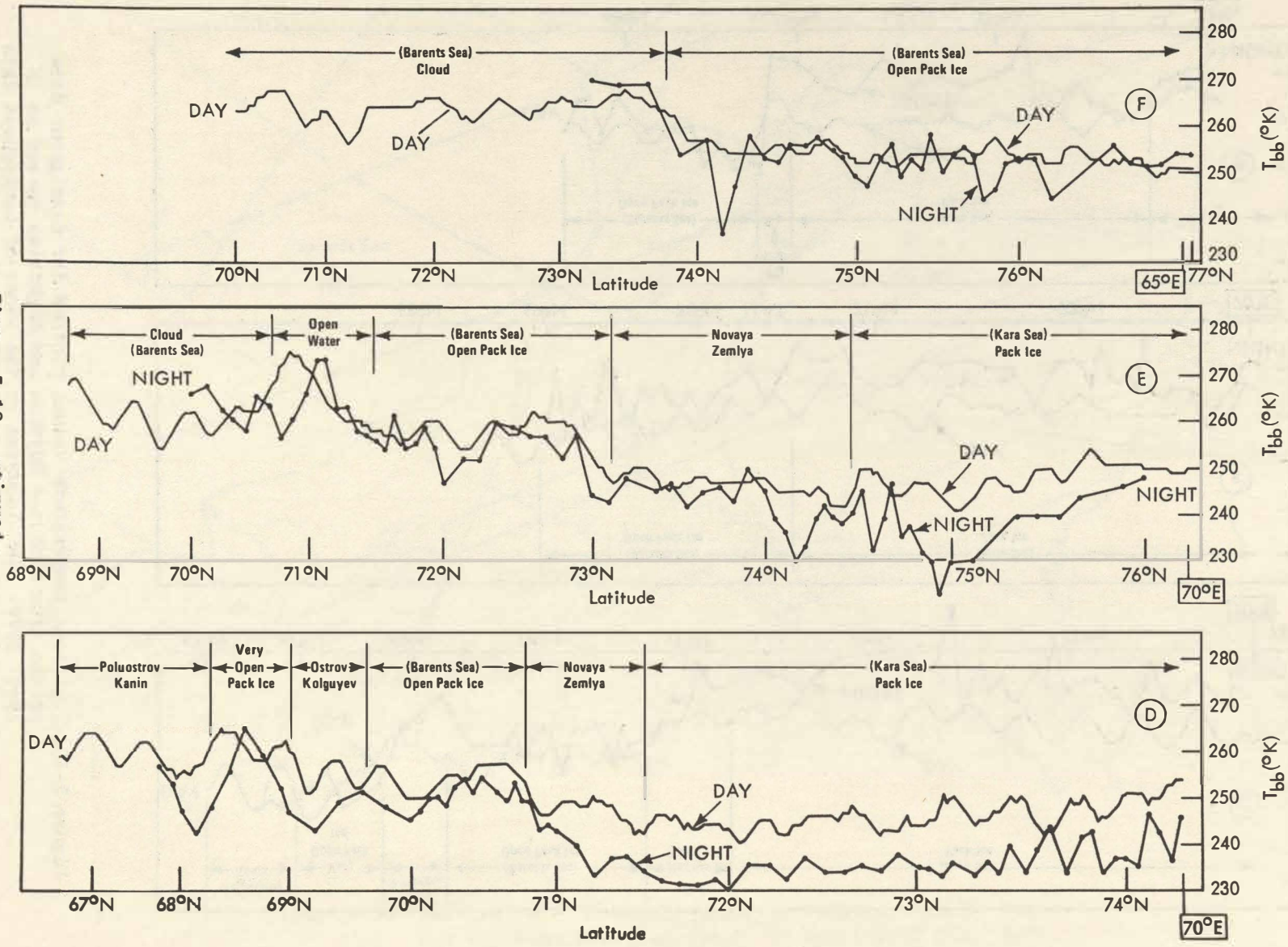

Figure 5-10 continued.

TABLE 5-1

DIURNAL VARIATIONS IN SURFACE TEMPERATURE
Nimbus Data, 18 April 1970

	Kara Sea (Pack Ice)			Barents Sea (Thin or Open Pack)		
	Mean T_{bb} (^{o}K)		ΔT_{bb}	Mean T_{bb} (^{o}K)		ΔT_{bb}
Scanline	Day	Night	($^{\circ}$K)	Day	Night	($^{\circ}$K)
A	250	239	11	254	252	2
B	248	241	7	251	246	5
C	245	237	8	252	250	2
D	246	236	10	254	250	4
E	247	237	10	257	254	3

(No average values were computed for data line F since this line did not intersect more than one feature.)

The temperatures in Table 5-1 show a number of interesting features. The first is that the effective blackbody temperatures are fairly uniform, both during the day and at night, over the uniform sea ice targets. More importantly, the data show an unambiguous difference in the ΔT_{bb} values computed for each of the seas. Based on interpretation of the ice coverage using the visible data, it may be tentatively concluded that the difference in the diurnal effect ΔT_{bb} is due to the differences in ice type. Over the compact pack ice of the Kara Sea, the surface temperatures of the ice respond strongly to the alternating cycle of daytime solar heating and nighttime radiative losses under clear sky conditions resulting in ΔT_{bb} values of 7 to 10°K. Over the thinner ice, or what is more probably open pack ice, of the Barents Sea, the large heat capacity of the exposed water surface prohibits large diurnal variations in surface temperature.

The second case provided less detailed information on the dependence of ΔT_{bb} or ice features and is useful primarily in further documenting the value of ΔT_{bb} for compact pack ice derived from the Kara Sea data. Subsequent to receipt of the digitized listings for the two passes over Baffin Bay, it was found that a number of the scan lines crossing the region were missing for the nighttime data (pass 147). As a result, the area for which both day and night time data are available is rather limited. The analysis was, therefore, confined to a narrow band oriented in a northwest-southeast direction centered at about 73.5°N and 70.5°W.

The IDCS photograph obtained during the daylight pass on 19 April (pass 151) over this region is shown in Figure 5-11. A map showing the general location of the band across this region and specific areas (labeled A to G) in the band within which data were analyzed is given in Figure 5-12. By comparing the photograph with the map, it is clear that the band of data selected for analysis lies in an area of pack ice of rather uniform reflectance characteristics, similar to that found over the Kara Sea for the 18 April case.

As in the previous case, mean values of T_{bb}(day) and T_{bb}(night) were obtained for each of the seven areas identified in the map in Figure 5-12. From these mean values, the diurnal differences in effective blackbody temperature, ΔT_{bb}, were computed. The results are shown in Table 5-2. The ΔT_{bb} values computed for this case are in essential agreement with the ones computed for the pack ice over the Kara Sea. The only exception is the value derived for region C which has a negative value. No explanation was found for this isolated anomalous case.

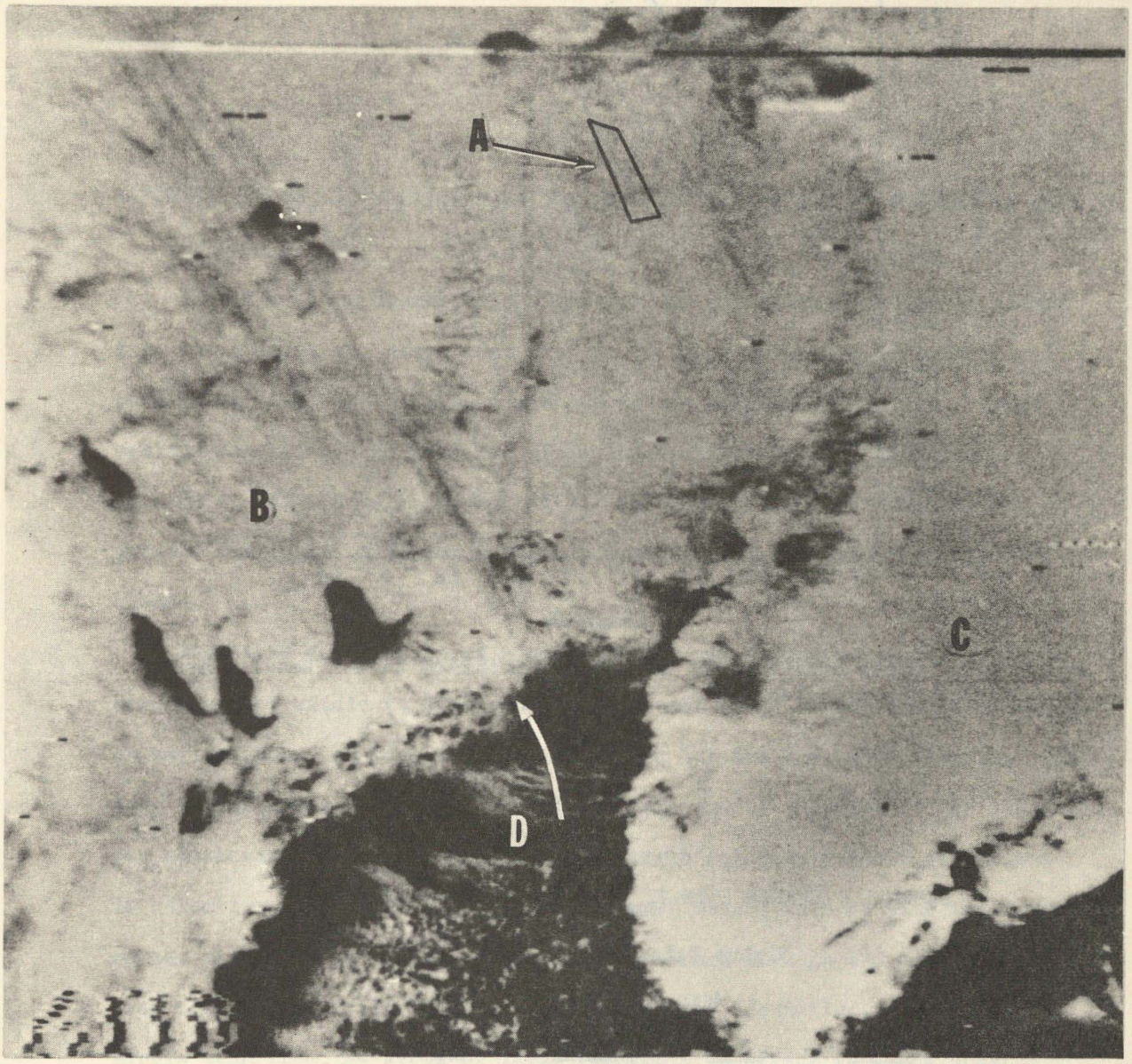

Figure 5-11 Nimbus-4 IDCS photograph showing Baffin Bay - Greenland area, 19 April 1970. Location of area shown in Figure 5-12 is indicated at A. Baffin Island is at B, Greenland at C, and ice edge at D.

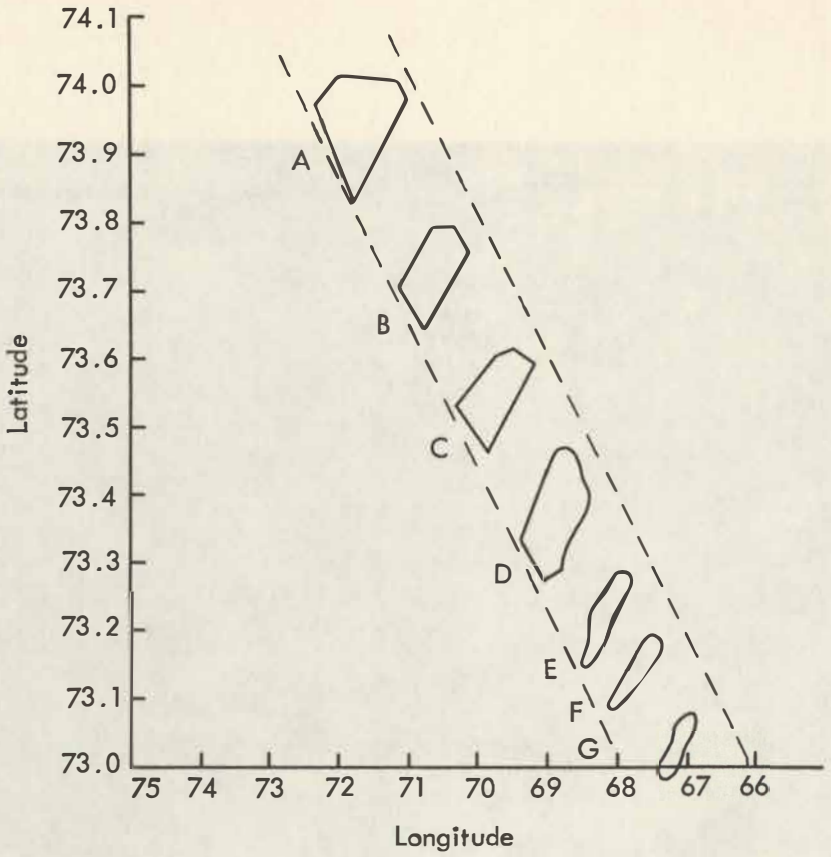

Figure 5-12 Areas analyzed for 19 April 1970 Nimbus data. Results are shown in Table 5-2.

TABLE 5-2

DIURNAL DIFFERENCE IN T_{bb} FOR THE BAFFIN BAY REGION

Nimbus Data, 19 April 1971

Area	Mean T_{bb} °K		ΔT_{bb}
	Day	Night	(^{o}K)
A	249	242	7
B	251	241	10
C	245	246	-1
D	251	242	9
E	249	241	8
F	247	238	9
G	246	240	6

6.

A DISCUSSION OF CLOUD DISCRIMINATION AND DIURNAL EFFECTS IN THERMAL IR DATA

The lack of an unambiguous signature for the discrimination of clouds from ice remains a persistent problem in the application of satellite photographic and infrared observations to the mapping of sea ice. Under certain conditions the presence of an undercast is readily discernable even in the digitized line scan data. In other situations even the use of pattern continuity will not result in positive discrimination of ice from clouds.

The ideal combination of conditions for cloud identification is to have bands of middle to high clouds over ocean areas during the late spring or early summer. During this period of sea ice breakup, the effective black body temperatures for the open pack ice near and at the edge of the ice fields are characteristically at or near 275^{o}K, with relatively small variations in effective black body temperatures between data points despite the large number of breaks in the ice field. The presence of high and middle clouds over such an ice field are almost unambiguously identified, even in a single scan line, as areas of large gradients in effective black body temperature bounding minimum temperatures that are uncharacteristic of open pack ice.

A good example of these conditions was illustrated in Section 5, Figure 5-4. In this figure, a number of scan lines measured on 17 July 1970 by the THIR of Nimbus 4 over the Beaufort Sea - Banks Island area are shown. The scan lines identified as A and B, intersect what undoubtedly are clouds over the open pack ice field in the Beaufort Sea. Over the areas of open

water and open pack, the point-to-point variations in effective black body temperatures are of the order of 2 to 3°K with the absolute temperatures ranging from about 270°K to 280°K. At the edge of the cloud, the effective blackbody temperatures show an uncharacteristically large gradient even between adjacent points. The absolute temperature falls to a minimum of less than 260°K, which is also uncharacteristic of open pack ice. This combination of temperature gradient and minimum temperature is associated with a cold land area or a cloud. Given this choice, it is clear that the characteristics of the spatial distribution of effective blackbody temperatures along a scan line can be used for the objective discrimination of clouds from ice.

At the other extreme of the cloud problem is the case of persistent fog or stratus over coastal regions. Here even the use of pattern continuity cannot result in an objective unambiguous discrimination of clouds. An example that illustrates the essential problems involved in objective identification of stratus is illustrated in the scan line analysis shown in Figure 4-4. In this example, the eastern portion of the scan line intersected what was subjectively interpreted from the corresponding photograph as low stratus over the Baffin Bay area. The effective blackbody temperature variations over the stratus have certain characteristics of note. At the edge of the cloud, the temperatures do exhibit a characteristic change in gradient. However, within the cloudy region the minimum temperatures are not excessively low in comparison with those over the adjacent ice fields; in fact, they are a few degrees higher. The relatively uniform point-to-point variations, or lack of variations, in temperature over most of the cloudy area are more characteristic of the temperature distribution over ice fields than of the type of clouds discussed previously.

Indeed, there is no objective clue that would indicate that the scan spots interpreted here as low stratus are not, in fact, associated with a relatively homogeneous ice field.

Another example of the characteristic temperature distribution over stratus is shown in Figure 6-1 (a and b). Although the DRSR image and the digitized data are from passes one day apart, it is doubtful that the ice edge moved significantly over this 24 hour period. As in the previous case, the effective temperature over the low stratus is characterized by the values which are lower than those found over the open water, and slightly higher than those found over the adjacent ice field. The difference in temperature over the ice and over the cloud is not sufficiently large to provide any form of positive discrimination. And, as in the previous case, the spatial distribution of temperatures over the cloudy region, together with the minimum temperatures, are indistinguishable from ice.

Faced with these problems it is clear that approaches towards cloud-ice discrimination based on simple threshold values of T_{bb} as discriminators would result in grossly overestimating the extent of ice coverage. The technique of forming multi-day composites, coupled with threshold discriminators using composited maximum temperatures, would be effective in discriminating transitory clouds from the more persistent ice field. However, persistent stratus will still be mapped as ice.

A possible approach towards minimizing the overestimation of pack ice coverage is to include in the discrimination scheme the use of diurnal temperature changes. It was shown in Section 5.2 that certain ice features have characteristic diurnal differences in effective blackbody temperatures.

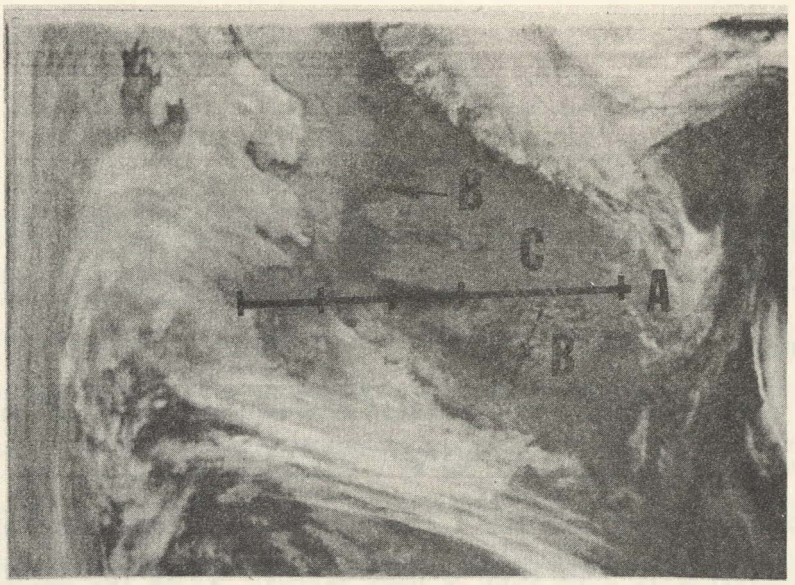

Figure 6-1a ITOS Nighttime DRSR image showing southern Baffin Bay area, 6 February 1971. Location of data swath plotted in Figure 6-1b is indicated at A. Ice edge is at B and stratus cloud at C.

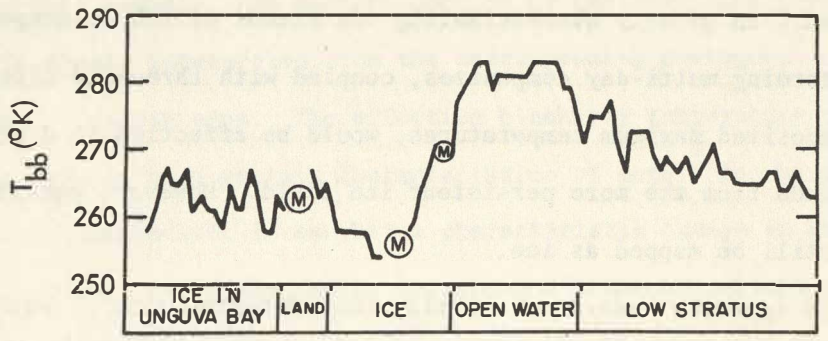

Figure 6-1b Analysis of digitized temperature values for data swath indicated in Figure 6-1a; ITOS-1 data, 7 February 1971.

For pack ice the difference is about 9°K, whereas for open pack the difference is substantially reduced to about 3°K. Over open water, there should be only a small systematic diurnal difference in the effective blackbody temperature. This is indicated in the analysis shown in Figure 5-10 (note Data Line E near 71.5°N). These characteristic values provide additional keys for the discrimination between different types of ice, as well as for the differentiation between open pack ice and open water. It is not inconceivable that the diurnal difference in effective blackbody temperature could also be used for discriminating persistent stratus from pack ice.

The type of stratus and fog found over the polar seas is generally formed as a result of advection of cold dry air from the land areas over the warmer waters, probably under stable conditions with the top of the fog or cloud layer capped by an inversion. As long as the synoptic-scale events which initially brought about the formation of this layer persist, it can be argued that the effective blackbody temperature of the layer, as measured from above by a satellite radiometer, should not undergo significant diurnal changes. For an optically thick cloud or fog layer, which these kinds of clouds appear to be, the effective blackbody temperature measured is essentially that of the cloud top or, in these cases, the temperature of the top of the inversion layer. As long as the cloud remains optically thick and the top of the inversion layer does not move substantially up or down, the effective blackbody temperature of the stratus should remain constant.

The ocean surface, unlike the land surface, does not undergo large diurnal variations in temperature, even at low latitudes under cloudless skies. Therefore, over the polar seas, the destabilization and subsequent dissipation of the stratus during daylight hours as a result of heating from below by the sea surface is unlikely. Furthermore, substantial modifications

of the optical thickness of the cloud top height resulting from direct absorption of sunlight by the cloud droplet is also unlikely considering the solar illumination conditions found over the polar regions during late spring. Thus, the most likely cause for the dissipation and formation of these persistent clouds is synoptic scale phenomena, which do not have a diurnal cycle. Given these arguments, it is not unreasonable to suggest the possibility that the diurnal differences in the effective temperature for persistent stratus is at best that of open water and at worst that of open pack. If this were in fact the case, the technique could be used in an effective scheme for differentiating fog and stratus from pack ice, even though both features have similar effective blackbody temperature characteristics at any given time.

The use of the diurnal difference in effective blackbody temperature in any overall scheme of sea ice mapping must of necessity be restricted only to those regions and those seasons for which alternating periods of darkness and sunlight, of whatever duration, occur in a 24-hour day. Additionally, the magnitude of the diurnal effect, being obviously dependent on the relative durations of the sunlit and darkness periods, will be seasonally and geographically dependent. Given these limitations, it is clear, therefore, that even when the temporal and spatial diurnal temperature difference signatures are fully developed and identified, they can serve at best as an additional tool in an overall mapping scheme combining the techniques of multi-day composites, maximum composite temperatures, and threshold temperature discriminators.

7. CONCLUSIONS

Thermal infrared measurements in the 10.5-12.5 μm spectral interval from the ITOS-1 Scanning Radiometer (SR) and the Nimbus-4 Temperature-Humidity Infrared Radiometer (THIR) provide a means for mapping gross ice boundaries during periods of polar darkness when observations in the visible portion of the spectrum are restricted. ITOS measurements transmitted in the direct readout mode are particularly useful because the DRSR imagery contains considerably less noise than the Nimbus imagery transmitted in the stored-data mode. Ice features of smaller scale can, therefore, be mapped from ITOS; in fact, if a sufficient thermal contrast exists, features smaller than the nominal resolution of the sensor (4.5 n.mi.) can be detected. The comparison between direct readout and stored data emphasizes the importance of noise-free measurements for ice mapping and other geophysical purposes, and demonstrates the potential for acquiring measurements of the desired quality through direct readout transmission. Since the higher resolution (0.5 n.mi.) thermal IR measurements from the forthcoming ITOS Very High Resolution Radiometer (VHRR) will be transmitted in a direct readout mode, it is anticipated that these data will have even greater application for ice surveillance.

In the analysis of the ITOS DRSR data, evidence was found indicating that the combined use of thermal IR and visible data can provide more information on ice conditions than can be deduced from either type of data alone. In observations of the Bering Sea, some areas were observed to have higher IR temperatures combined with lower visible reflectances; these areas are deduced to consist of lesser ice concentrations. On the other hand, a higher IR temperature was measured in another area where no significant

decrease in reflectance was observed in the visible data; because of the high reflectance, this area is deduced to consist of either thinner ice or ice with less snow cover, but not a lesser ice concentration.

The densitometric analysis performed in this study suggests that direct readout photofacsimile data, when properly normalized, may provide crude quantitative information on ice distributions. For the data sample examined, a linear adjustment of densities, normalized to the density corresponding to the ocean surface under clear-sky conditions, enabled density values from different orbital passes to be meaningfully compared. The finding of a unique relationship between density classes and three types of ice features (i.e. ice-free, pack ice, and ice cap) is significant if objective techniques are to be developed for interpretation of photofacsimile data.

The analysis of nighttime data in the digitized format indicates, in general, that the 5-level mapping scheme developed previously using Nimbus HRIR data is applicable to ITOS data as well. Using this scheme, the ice edge in Baffin Bay could be mapped from a sample of five ITOS passes during the winter and early spring season. As was also found with the earlier Nimbus data, however, the prevalence of stratus clouds over open water areas can obscure the ice edge at times. Through a limited calibration against sea-surface temperature and a comparison with nearly concurrent Nimbus data, it is concluded that the absolute ITOS temperature values analyzed in this study are $5^{o}K$ or more too high. However, a decrease in temperature from February to March observed in both the ITOS data and the sea surface temperature reports gives further evidence that the relative temperature values measured by ITOS are useful.

The availability of Nimbus data during the Arctic summer season provided the first opportunity to investigate the application of high resolution daytime thermal IR measurements for mapping sea ice. The results of

the analysis of these data indicate that during the summer season little or no temperature contrast exists between ice and water; perhaps the ice is not as thick or solid during the summer and may be covered with melt water. Although the temperature difference may be sufficient to be mapped in full-resolution digitized data listings, the ice edge is often not detectable in the film-strip presentation. Thus, if ice during summer, daytime periods is to be mapped from photofacsimile data, the selection of appropriate gray levels to be displayed must be carefully considered.

The availability of Nimbus data during the spring season also provided an opportunity to compare daytime and nighttime thermal IR measurements. In analyses performed from a rather limited data sample, the diurnal difference in effective blackbody temperature appears to be correlated with the thickness of the ice and/or the percentage of ice cover, or more likely a combination of both of these important aspects of the ice field, Specifically, it was found that for close pack ice the diurnal range of temperature was of the order of 9^{o} to 10^{o}K, a value characteristically different from the value for thin and broken pack ice, which was of the order of 3^{o}K. These differences are obviously geographically and seasonally dependent. Further investigations must be conducted to establish their use as signatures to aid in the mapping of ice features.

Although no analysis of the diurnal difference in temperature was made for cloudy regions because of problems in obtaining digitized data, it appears that this parameter might be useful, as well, for the objective discrimination between ice and stratus cloud. This hypothesis must be tested using a larger data sample.

REFERENCES

Aber, P.G. and E. Vowinckel, 1971: Evaluation of North Water Spring Ice Cover from Satellite Photographs, Publication in Meteorology No. 101, Dept. of Meteorology, McGill University, Montreal, 23 pp.

Anderson, R.K. and A.H. Smith, 1971: "Infrared", Supplement to Application of Meteorological Satellite Data in Analysis and Forecasting, ESSA Technical Report NESC 51, National Environmental Satellite Service.

Barnes, J.C., D.T. Chang and J.H. Willand, 1969: Use of Satellite High- Resolution Infrared Imagery to Map Arctic Sea Ice, Final Report under Contract No. N62306-68-0276 to Naval Oceanographic Office, Allied Research Associates, Inc.

Barnes, J.C., D.T. Chang and J.H. Willand, 1970: Improved Techniques for Mapping Sea Ice from Satellite Infrared Data, Final Report under Contract No. E-67-70(N) to National Oceanic and Atmospheric Administration, Allied Research Associates, Inc.

Barnes, J.C., D.T. Chang, and J.H. Willand, 1972: "Image Enhancement Techniques for Improving Sea Ice Depiction in Satellite Infrared Data," Journal of Geophysical Research; Oceans and Atmospheres Edition, 77(3), pp. 453-462.

Keegan, T.J., 1972: "An Evaluation of Direct Readout Infrared Data" Mon. Wea. Rev, 100 (2) pp. 117 - 125

List, R.J., 1966: Smithsonian Meteorological Tables, sixth revised edition, Smithsonian Institution, Washington, D.C., pp. 497-505.

McClain, E.P. and M.D.Baliles, 1971: "Sea Ice Surveillance from Earth Satellites," Mariners Weather Log, Vol. 15, No. 1, pp. 1-4.

Navy Hydrographic Office, 1958: Oceanographic Atlas of the Polar Seas, Part II - Arctic, pp. 45-93, Washington, D.C.

Naval Oceanographic Office, 1971: Birds Eye 2-71, 3-15 February 1971, Publication IR No. 71-9, Washington, D.C.

Sabatini, R.R. (editor), 1970: The Nimbus IV User's Guide, prepared by the Nimbus Project, Goddard Space Flight Center, National Aeronautics and Space Administration.

Smith, W.L., P.K. Rao, R. Koffler, and W.R. Curtis, 1970: "The Determination of Sea-Surface Temperature From Satellite High Resolution Infrared Window Measurements", Mon. Wea. Rev., 48,604-611